CH₃CO + O₂ + M (M = He, N₂) Reaction Rate Coefficient Measurements and Implications for the OH Radical Product Yield

Vassileios C. Papadimitriou,[†,‡,§,∥] Emmanuel S. Karafas,[§] Tomasz Gierczak,[†,‡,⊥] and James B. Burkholder*,[†]

[†]Earth System Research Laboratory, Chemical Sciences Division, National Oceanic and Atmospheric Administration, 325 Broadway, Boulder, Colorado 80305, United States

[‡]Cooperative Institute for Research in Environmental Sciences, Colorado University, 216 UCB, Boulder, Colorado 80309, United States

[§]Laboratory of Photochemistry and Chemical Kinetics, Department of Chemistry, University of Crete, Vassilika Vouton, 71003 Heraklion, Crete, Greece

ABSTRACT: The gas-phase CH₃CO + O₂ reaction is known to proceed via a chemical activation mechanism leading to the formation of OH and CH₃C(O)OO radicals via bimolecular and termolecular reactive channels, respectively. In this work, rate coefficients, k, for the CH₃CO + O₂ reaction were measured over a range of temperature (241−373 K) and pressure (0.009−600 Torr) with He and N₂ as the bath 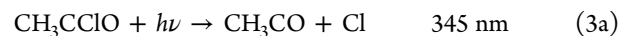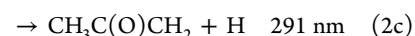gas and used to characterize the bi- and ter-molecular reaction channels. Three independent experimental methods (pulsed laser photolysis−laser-induced fluorescence (PLP−LIF), pulsed laser photolysis−cavity ring-down spectroscopy (PLP−CRDS), and a very low-pressure reactor (VLPR)) were used to characterize $k(T,M)$. PLP−LIF was the primary method used to measure $k(T,M)$ in the high-pressure regime under pseudo-first-order conditions. CH₃CO was produced by PLP, and LIF was used to monitor the OH radical bimolecular channel reaction product. CRDS, a complementary high-pressure method, measured $k(295\ K,M)$ over the pressure range 25−600 Torr (He) by monitoring the temporal CH₃CO radical absorption following its production via PLP in the presence of excess O₂. The VLPR technique was used in a relative rate mode to measure $k(296\ K,M)$ in the low-pressure regime (9−32 mTorr) with CH₃CO + Cl₂ used as the reference reaction. A kinetic mechanism analysis of the combined kinetic data set yielded a zero pressure limit rate coefficient, $k_{int}(T)$, of $(6.4 \pm 4) \times 10^{-14} \exp((820 \pm 150)/T)$ cm³ molecule⁻¹ s⁻¹ (with $k_{int}(296\ K)$ measured to be $(9.94 \pm 1.3) \times 10^{-13}$ cm³ molecule⁻¹ s⁻¹), $k_0(T) = (7.39 \pm 0.3) \times 10^{-30} (T/300)^{-2.2\pm0.3}$ cm⁶ molecule⁻² s⁻¹, and $k_\infty(T) = (4.88 \pm 0.05) \times 10^{-12} (T/300)^{-0.85\pm0.07}$ cm³ molecule⁻¹ s⁻¹ with $F_c = 0.8$ and M = N₂. A He/N₂ collision efficiency ratio of 0.60 ± 0.05 was determined. The phenomenological kinetic results were used to define the pressure and temperature dependence of the OH radical yield in the CH₃CO + O₂ reaction. The present results are compared with results from previous studies and the discrepancies are discussed.

1. INTRODUCTION

The gas-phase reaction of the acetyl radical, CH₃CO, with molecular oxygen, O₂, written simply as

$$CH_3CO + O_2 + M \rightarrow products \qquad (1)$$

has been shown previously to have a temperature- and pressure-dependent reaction rate coefficient, $k_1(T,M)$, that is consistent with a chemical activation reaction mechanism,[1] as shown in Scheme 1.

The energized CH₃C(O)OO* reaction intermediate can decompose back to reactants or proceed to reaction products through a pressure-independent channel (often referred to as a bimolecular channel) to form an OH radical or to a peroxyacetyl radical stabilized by collision with the bath gas (referred to as a pressure-dependent or termolecular channel). This chemical activation mechanism is analogous to that of the OH + CO reaction that proceeds through an energized HOCO* intermediate. (See Sander et al.[2] and references

Scheme 1

CH₃CO + O₂ $\underset{k_{-1}}{\overset{k_1}{\rightleftarrows}}$ CH₃C(O)OO* $\overset{k_2}{\longrightarrow}$ OH + Product

k_3 ↓ +M

CH₃C(O)OO

within.) The phenomenological rate coefficients (kinetic measurements based on the observed loss of the CH_3CO radical or the formation of OH or $CH_3C(O)OO$ radical products) for reaction 1 are, therefore, expected to display a combination of bimolecular and termolecular temperature and pressure-dependent behavior. Note that in the zero-pressure limit, that is, only bimolecular behavior, the OH yield in Scheme 1 is expected to be unity, while in the high-pressure limit it is expected to be zero.

Reaction 1 and its mechanism is of general kinetic interest because of its unique reaction product yield as a function of temperature and pressure, while it also plays an important role in tropospheric chemistry. Reaction 1 is of particular importance because the formation of the acetylperoxy radical, $CH_3C(O)O_2$, leads to the formation of peroxyacetyl nitrate (PAN, $CH_3C(O)O_2NO_2$), which is an atmospheric reservoir for NO_x (NO_x = NO + NO_2). PAN plays an important role in the long-range transport of NO_x, which impacts ozone production throughout the troposphere as well as regional air quality.[3,4]

The kinetics of reaction 1 has been the subject of numerous experimental and theoretical studies.[5−12] The experimental studies have covered a range of temperature and pressure and have applied both absolute and relative rate kinetic methods. Overall, the existing kinetic data are in reasonable agreement. (The individual studies are discussed in the Results and Discussion section.) Although there has been significant effort to measure the pressure and temperature dependence of the phenomenological rate coefficient for reaction 1, the mechanism is, however, still not characterized well enough to reliably evaluate the temperature and pressure dependence of the OH radical product yield. The lack of experimental data in the low-pressure regime as well as the limited level of agreement among the existing data particularly hampers a kinetic analysis of the OH product yield. Theoretically, Maranzana et al.[13] and Carr et al.[7] have used master equation simulations to evaluate the reaction mechanism. The OH yield was found to be a sensitive function of the $CH_3C(O)OO^*$ collisional energy transfer (i.e., stabilization) parametrization, making it difficult to predict the pressure and temperature dependence of the OH yield and differentiate between existing experimental data. Because of existing discrepancies in both high-and low-pressure reaction rate coefficient results and reports of the OH radical product yield, further experimental studies are warranted.

In this work, three independent experimental methods (pulsed laser photolysis-laser-induced fluorescence (PLP−LIF), pulsed laser photolysis−cavity ring-down spectroscopy (PLP−CRDS), and a very low-pressure reactor (VLPR) technique) were combined to measure rate coefficients for the $CH_3CO + O_2$ reaction. Rate coefficients were measured over the temperature range 241 to 373 K and over the pressure range 0.009 to 600 Torr (He and N_2 bath gases). The phenomenological rate coefficient data are used to evaluate the pressure and temperature dependence of the OH radical yield based on Scheme 1. The use of different bath gases enabled a further evaluation of the reaction mechanism and collisional energy transfer efficiency used in master equation simulations.[13] The present rate coefficient and OH yield results are compared with previous results, and the discrepancies are discussed.

2. EXPERIMENTAL DETAILS

The rate coefficient, k, for the gas-phase $CH_3CO + O_2$ reaction was measured using three independent experimental methods:

PLP−LIF, PLP−CRDS, and VLPR. The PLP−LIF method was used for the majority of the kinetic measurements performed at total pressures >10 Torr. CH_3CO radicals were produced via pulsed UV laser photolysis (described later), and LIF was used to measure the OH radical temporal profile. The CRDS method used pulsed UV laser photolysis to produce the CH_3CO radical while monitoring the temporal CH_3CO radical absorption at 532 nm. CRDS measurements were performed at 295 K over a 25 to 600 Torr (He) pressure range. The VLPR method used a continuous-flow reactor coupled to a quadru-pole mass spectrometer (QMS) that was used to monitor the competitive reactive loss of Cl_2 and O_2 due to reaction with the CH_3CO radical. The VLPR measurements were performed at 296 K with total pressures in the range 9 to 32 mTorr (He). The PLP−LIF,[14,15] PLP−CRDS,[16,17] and VLPR−QMS[18−22] apparatuses have been used extensively previously and are described in detail elsewhere. The CH_3CO radical source chemistry used in the present study as well as experimental details and methods relevant to the present work are described separately later.

2.1. CH_3CO Radical Sources. CH_3CO radicals were produced in the LIF and CRDS kinetic measurements by pulsed UV laser photolysis. In the VLPR measurements the CH_3CO radical was produced by chemical reaction. Acetone ($CH_3C(O)CH_3$) and acetyl chloride (CH_3CClO) were used as photolytic precursors

$$CH_3C(O)CH_3 + h\nu \rightarrow CH_3CO + CH_3 \qquad 338\ nm \qquad (2a)$$

$$\rightarrow 2CH_3 + CO \qquad 298\ nm \qquad (2b)$$

$$\rightarrow CH_3C(O)CH_2 + H \qquad 291\ nm \qquad (2c)$$

$$CH_3CClO + h\nu \rightarrow CH_3CO + Cl \qquad 345\ nm \qquad (3a)$$

$$\rightarrow CH_3 + ClCO \qquad 326\ nm \qquad (3b)$$

where the photodissociation threshold wavelengths were calculated using the heats of formation from Sander et al.[2] Photolysis of $CH_3C(O)CH_3$ and CH_3CClO at 248 nm was used in both the LIF and CRDS studies, while 280 nm photolysis of $CH_3C(O)CH_3$ was also used in the LIF study.

The CH_3CO radical quantum yield, $\Phi_\lambda(CH_3CO)$, in the photolysis of $CH_3C(O)CH_3$ at 248 and 280 nm is reasonably well established.[6,17,23−25] $\Phi_{248}(CH_3CO)$ has been shown to be pressure-dependent with an increasing value with increasing pressure. Over the range of pressures used in the present work, 10−600 Torr, $\Phi_{248}(CH_3CO)$ varies from 0.55 to 0.81.[17] The photolysis of $CH_3C(O)CH_3$ at 280 nm has a unit CH_3CO quantum yield and is independent of pressure.[6,26] To the best of our knowledge, $\Phi_{248}(CH_3CO)$ in the photolysis of CH_3CClO has not been reported in the literature. In the course of our work, $\Phi_{248}(CH_3CO)$ was estimated to be ∼0.55. We note here that knowledge of $\Phi_\lambda(CH_3CO)$ is not required for the determination of $k(T,P)$, but it does enable an estimate of the radical concentrations used in the kinetic measurements. The $CH_3C(O)CH_3$ and CH_3CClO concentrations were varied over the course of the study between 5 and 10×10^{15} molecules cm^{-3}, and the photolysis laser fluence was varied over the range 5 to 20 mJ cm^{-2} $pulse^{-1}$. This corresponds to initial CH_3CO radical concentrations, $[CH_3CO]_0$, in the range $(5-10) \times 10^{11}$ molecules cm^{-3}.

Two CH_3CO radical source reactions were used in the VLPR experiments

$$F + CH_3CHO \rightarrow HF + CH_3CO \qquad (4a)$$

$$\rightarrow HF + CH_2CHO \qquad (4b)$$

$$Cl + CH_3CHO \rightarrow HCl + CH_3CO \qquad (5a)$$

$$\rightarrow HCl + CH_2CHO \qquad (5b)$$

where $k_4(298\ K) = 1.4 \times 10^{-10}\ cm^3\ molecule^{-1}\ s^{-1}$[10,27] and $k_5(298\ K) = 8 \times 10^{-11}\ cm^3\ molecule^{-1}\ s^{-1}$.[28] Reaction 4 produces both CH_3CO and CH_2CHO radicals with product yields of ~65 and ~35%, respectively.[10] Niki et al.[29] reported that the Cl atom initiated reaction yields >99% CH_3CO radicals, while Bartels et al.[30] report a yield of >93%. A CH_3CO yield of unity in the Cl atom reaction was used in our data analysis. (The sensitivity to the product yield is discussed in the Error Analysis section.) The extent of the source reaction and radical formation was verified experimentally by monitoring the loss of the CH_3CHO precursor at $m/e = 43$ and Cl atoms at $m/e = 35$. The concentration range for CH_3CHO was $(0.1-1.7) \times 10^{14}$ molecules cm^{-3}, while the initial CH_3CO radical concentration was between $(2.0$ and $3.5) \times 10^{11}$ molecules cm^{-3}. Cl_2 and O_2 reactant concentrations were in the range $(0.3-5.0) \times 10^{13}$ and $(2.0$ to $3.0) \times 10^{14}$ molecules cm^{-3}, respectively.

Halogen atoms were produced in a low-power microwave discharge side arm. Dilute mixtures, 5% F_2 and 10% Cl_2 in He, were passed through a quartz discharge tube enclosed within a 2.45 GHz Evenson microwave cavity operating at 35 W. The discharge effluent mixed with CH_3CHO in the VLPR reactor. Initial halogen atom concentrations were ~2.5×10^{12} atom cm^{-3}.

2.2. Pulsed Laser Photolysis−Laser-Induced Fluorescence. The PLP−LIF apparatus consists of three main components: (1) the LIF reactor where reaction takes place and OH radicals are detected, (2) pulsed photolysis lasers used to produce CH_3CO radicals, and (3) a pulsed probe laser used to excite OH. The LIF reactor was temperature-regulated by circulating fluid from a temperature-regulated bath through its jacket. The gas temperature in the reaction zone of the reactor was measured using a retractablue thermocouple, accurate to ±0.5 K.

OH radical temporal profiles were recorded by measuring its fluorescence following excitation of the $A^2\Sigma^+(v = 1) \leftarrow X^2\Pi$ ($v = 0$) transition at 282 nm with the frequency-doubled output of a Nd:YAG pumped dye laser. OH fluorescence from the $A^2\Sigma^+ \rightarrow X^2\Pi$ ($v' \rightarrow v''$ 0−0 and 1−1) transitions was collected using a pair of convex lenses, passed through a 308 nm band-pass filter (20 nm fwhm bandwidth) and detected by a photo-multiplier tube (PMT). The PMT signal was averaged for 100 laser shots with a gated charge integrator. OH radical temporal profiles were obtained by varying the delay between the photolysis laser and the probe laser over the range 0.01−50 ms.

Kinetic experiments were performed under pseudo-first-order conditions in the CH_3CO radical, $[O_2] > 1000 \times [CH_3CO]$, over a range of temperature (241−373 K) and pressure (10−200 Torr) with He or N_2 bath gases. The OH radical temporal profiles were described by a biexponential expression

$$S_{OH}(t) = C[\exp(-k'_{loss}t) - \exp(-k'_{rise}t)] \qquad (I)$$

where $S_{OH}(t)$ is the OH radical fluorescence signal at time t, C is a constant that is proportional to $\theta[CH_3CO]_0$ where θ is the OH radical yield in reaction 1, and k'_{loss} and k'_{rise} are the pseudo-first-order rate coefficients for the loss and formation of the OH radical, respectively. The rate of the initial rise in the OH radical concentration is a measure of the pseudo-first-order rate coefficient for reaction 1, $k'_{rise} = k_1[O_2]$. $k_{loss} = k'_2 + k_d$, where k'_2 is the pseudo-first-order rate coefficient for the reaction of OH with the CH_3CO precursor and k_d is the first-order loss of OH radicals due to diffusion out of the reaction volume. k'_{loss} values were in the range 100 to 3000 s^{-1}. k'_{loss} was primarily determined by the reaction of OH with the precursor molecule. A nonlinear least-squares fit of the OH temporal profile to eq I was used to obtain k'_{rise} at different O_2 concentrations. The O_2 concentration was varied over the range $(1.60-22.5) \times 10^{15}$ molecules cm^{-3}. $k_1(T,M)$ at a given temperature and pressure was determined from a linear least-squares fit of k'_{rise} versus $[O_2]$.

2.3. Cavity Ring-Down Spectroscopy. CRDS was used to measure the CH_3CO radical temporal profile following its pulsed laser photolysis production in the presence of excess O_2. The CH_3CO absorption spectrum between 490 and 660 nm is continuous with an absorption cross section, σ, of $(1.1 \pm 0.2) \times 10^{-19}\ cm^2\ molecule^{-1}$ at 532 nm.[16] The CRDS ring-down time constant, τ, is related to the absorption coefficient, α (cm^{-1}), at time t by

$$\alpha_t = [CH_3CO]_t \sigma_{CH_3CO} = \frac{1}{c}\frac{d}{L_s}\left(\frac{1}{\tau_t} - \frac{1}{\tau_0}\right) \qquad (II)$$

where $[CH_3CO]$ is the CH_3CO radical concentration, σ_{CH_3CO} is its absorption cross section ($cm^2\ molecule^{-1}$) at the CRDS probe wavelength, λ, d is the optical cavity path length (cm), L_s is the path length (cm) of the absorbing species, c is the speed of light, and τ_τ and τ_0 are the ring-down time constants (s) with and without the absorber present, respectively. The probe beam for the CRDS measurements at 532 nm was taken from a frequency-doubled Nd:YAG laser. The mirror reflectivity at 532 nm was ~99.995%, which gives a value for τ_0 of ~80 μs for a cavity path length of ~1 m. A crossed PLP−CRDS setup was used with the reactor mounted midway between the CRD mirrors. The Pyrex reactor was 25 cm long with a diameter of 5 cm.[16] The overall optical cavity length, d, was 96 cm and L_s = 4.7 cm.

Rate coefficients were measured at 295 K over the pressure range 25 to 600 Torr (He) under pseudo-first-order conditions in CH_3CO, $[CH_3CO] \ll [O_2]$. The photolysis laser fluence was varied over the range 3−15 mJ cm^{-2} $pulse^{-1}$, and the initial CH_3CO radical concentration was in the range $(3-7) \times 10^{12}$ molecules cm^{-3}. The simultaneous kinetics and ring-down (SKaR) technique, which is most applicable under conditions where the loss of CH_3CO occurred on the time scale of the ring-down time constant, was used in the measurement of $k_1(295\ K,M)$. Details of the SKaR method are described elsewhere.[31,32] Under first-order loss conditions, the ratio of the ring-down profile with reactive loss to that measured without is given by

$$R(t) = \exp\left[-\left(\frac{c\alpha_0}{k'}\right) \times \{1 - \exp(-k't)\}\right] \qquad (III)$$

The experimentally determined $R(t)$ was calculated from the average of 20 individual decay profiles measured with and without reactive loss. A nonlinear least-squares fit of $\ln(R(t))$ versus time was used to obtain k'. k' was determined at various values of $[O_2]$, where at least eight different O_2 concentrations

in the range $(1.60-22.5) \times 10^{15}$ molecules cm^{-3} were used at each pressure. k_1(295 K,M) was obtained from a linear least-squares fit of k' versus [O$_2$].

2.4. Very Low-Pressure Reactor. Rate coefficients for the reaction of CH$_3$CO + O$_2$ at 296 K were measured using VLPR and a competitive reaction method in the ~9 to 32 mTorr total pressure regime. CH$_3$CO + Cl$_2$ was used as the reference reaction in these experiments. The key components of the VLPR system include (1) a jacketed Pyrex Knudsen reactor with three capillary gas inlets, (2) 10 L Pyrex storage bulbs used to supply the Knudsen reactor with a constant flow of reactant gases through calibrated buffer volumes and capillaries, (3) a microwave discharge source used to produce F or Cl atoms, and (4) a QMS used to detect reactants and stable reaction products. The Knudsen reactor (V_{cell}, 290 cm^3) was internally coated with a thin layer of Teflon (FEP 121-A). The reactor temperature was regulated to ±0.1 K by circulating water or methanol through the reactor jacket.

k_1(296 K,M) was measured relative to the CH$_3$CO + Cl$_2$ reaction under constant reactant flow conditions. The changes in the O$_2$ and Cl$_2$ concentration, in the presence and absence of the CH$_3$CO radical, in experiments performed using the Cl + CH$_3$CHO reaction as the CH$_3$CO radical source are given by

$$\Delta[O_2]k_{esc}^{O_2} = k_1[CH_3C(O)]_r[O_2]_r \tag{IV}$$

$$\Delta[Cl_2]k_{esc}^{Cl_2} = k_{ref}[CH_3C(O)]_r[Cl_2]_r \tag{V}$$

where $k_{esc}^{O_2}$ and $k_{esc}^{O_2}$ are the first-order escape rate coefficients for O$_2$ and Cl$_2$. The concentration of species X within the Knudsen reactor ([CH$_3$CO]$_r$, [O$_2$]$_r$, and [Cl$_2$]$_r$) is proportional to the intensity of its parent or prominent mass spectrometric (MS) peak and is given by

$$[X]_r = F_X(k_{esc}^X V_{cell})^{-1} = I_X(\alpha_X V_{cell} k_{esc}^X)^{-1} \tag{VI}$$

where I_X is the MS signal intensity, α_X is a flow rate calibration factor (s molecule^{-1}), and F_X is the reactant flow rate (molecule s^{-1}) (determined in separate experiments as described elsewhere).[18] The escape rate coefficient, k_{esc}^X, is determined experimentally in separate experiments by monitoring the first-order decay of a species mass spectrometric signal after halting the gas flow. (See Stefanopoulos et al.[22] for further details.) k_{esc}^X is given by $A_{esc} \times (T/m_X)^{1/2}$ (s^{-1}), where m_X is the molecular weight of species X and A_{esc} is the escape constant defined by the reactor volume, geometry, and escape orifice size. Linear least-squares fits of k_{esc}^X versus $(T/m_X)^{1/2}$ for various m_X are used to determine the escape constant. For V_{cell} = 290 cm^3 and a 1 mm escape orifice, which was used in the majority of the present experiments, A_{esc} was measured to be 5.0×10^{-2} s^{-1}. Note that the escape rate coefficient is not used in the kinetic analysis but is useful for defining reactant and product residence times in the reactor. The residence times for F, Cl, CH$_3$CO, O$_2$, and Cl$_2$ were 5.07, 6.88, 7.62, 6.58, and 9.72 s, respectively. Typical molecular flow rates were ~10^{16} and ~4 × 10^{16} molecule s^{-1} for the Cl$_2$ and F$_2$ mixtures, respectively, ~(5–100) × 10^{14} molecule s^{-1} for the Cl$_2$/O$_2$ mixture and ~(4–40) × 10^{14} molecule s^{-1} for CH$_3$CHO.

Rearranging and combining eqs IV, V, and VI yields

$$\left(\frac{I_0^{O_2}}{I_r^{O_2}} - 1\right)\sqrt{\frac{m_{Cl_2}}{m_{O_2}}} = \frac{k_1}{k_{ref}}\left(\frac{I_0^{Cl_2}}{I_r^{Cl_2}} - 1\right) \tag{VII}$$

where $I_0^{O_2}$ and $I_r^{O_2}$ are the measured mass spectral intensities of O$_2$ (m/e: 32) in the absence and presence of CH$_3$CHO in the Knudsen reactor, respectively; $I_0^{Cl_2}$ and $I_r^{Cl_2}$ are the corresponding mass spectral intensities for Cl$_2$ (m/e: 70); and k_1 and k_{ref} are the rate coefficients for the O$_2$ + CH$_3$CO and Cl$_2$ + CH$_3$CO reactions, respectively, where $k_{ref} = (3.0 \pm 0.5) \times 10^{-11}$ cm^3 molecule^{-1} s^{-1}.[32] The k_1/k_{ref} rate coefficient ratio was obtained as the slope from a linear least-squares analysis of $((I_0^{O_2}/I_r^{O_2}) - 1)(m_{Cl_2}/m_{O_2})^{1/2}$ versus $((I_0^{Cl_2}/I_r^{Cl_2}) - 1)$.

When the F + CH$_3$CHO reaction was used as the CH$_3$CO radical source, the data analysis was similar, although the production of the CH$_2$CHO radical in the source reaction and its reaction with O$_2$ and Cl$_2$

$$CH_2CHO + O_2 \rightarrow products \tag{6}$$

$$CH_2CHO + Cl_2 \rightarrow products \tag{7}$$
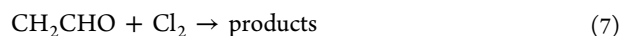
was included in the derived formulas. Abstraction of the carbonyl H atom is the major reaction channel in reaction 4 with a CH$_3$CO radical yield of 65%, while the CH$_2$CHO radical product channel accounts for the balance of the reaction, [CH$_2$CHO]/[CH$_3$CO] = 0.54.[10] Under constant reactant flows, the change in O$_2$ and Cl$_2$ concentration is then given by

$$\Delta[O_2]k_{esc}^{O_2} = k_1[CH_3C(O)]_r[O_2]_r + k_6[CH_2CHO]_r[O_2]_r \tag{VIII}$$

$$\Delta[Cl_2]k_{esc}^{Cl_2} = k_{ref}[CH_3C(O)]_r[Cl_2]_r + k_7[CH_2CHO]_r[Cl_2]_r \tag{IX}$$

which leads to

$$\left(\frac{I_0^{O_2}}{I_r^{O_2}} - 1\right)\sqrt{\frac{m_{Cl_2}}{m_{O_2}}} = \frac{k_1 + 0.54k_6}{k_{ref} + 0.54k_7}\left(\frac{I_0^{Cl_2}}{I_r^{Cl_2}} - 1\right) \tag{X}$$

The overall significance of the loss of O$_2$ and Cl$_2$ due to reaction with CH$_2$CHO, using the literature value for the reaction of CH$_2$CHO with O$_2$ and an upper-limit for the corresponding reaction with Cl$_2$, is described in the Results and Discussion section. All kinetic measurements were performed with an ionization electron energy of 19 eV to suppress Cl$_2$ and O$_2$ fragmentation within the ion source.

2.5. Materials. He (UHP, 99.999%), N$_2$ (UHP, 99.99%), and O$_2$ (UHP, 99.99%) were used as supplied. The CH$_3$C(O)CH$_3$ (>99.9%), CH$_3$ClO (>99%), CH$_3$I (>99%), and (CH$_3$CHO, >99.5%) samples were degassed via several freeze–pump–thaw cycles. The photolytes and reactants were added to the reactors from dilute gas mixtures prepared manometrically off-line. Infrared absorption spectra of the mixtures verified that the mixtures were stable over the course of the study. Gas-flow rates were such that the reaction mixture in the LIF or CRDS reactor was flushed out between photolysis laser pulses. Linear gas flow velocities in the LIF reactor were in the range 5–20 cm s^{-1}. The temperature of the gas within the reaction volume of the reactor was measured using a retractable thermocouple. Pressures were measured using 10, 100, and 1000 Torr capacitance manometers. In the VLPR measurements, 5% F$_2$/He, 10.2% Cl$_2$/He, 66% CH$_3$CHO/He, and 11% Cl$_2$/O$_2$ mixtures were used. Samples were admitted into the Knudson reactor from separate ~150 cm long, ~0.9 mm i.d. capillaries. The reactor pressure varied over the course of an experiment between ~9 and 12 mTorr and 20 and 32 mTorr when using the Cl + CH$_3$CHO and F + CH$_3$CHO sources,

respectively. Uncertainties presented throughout the paper are at the 2σ (95% confidence interval) unless stated otherwise.

3. RESULTS AND DISCUSSION

The kinetic results obtained using the three complementary techniques are presented separately. The phenomenological rate coefficient data are combined and a temperature- and pressure-dependent kinetic analysis that includes the bimolecular and termolecular falloff behavior (Scheme 1) for reaction 1 is then presented. The present kinetic results are compared with results from previous studies and the observed discrepancies in the high and low-pressure regimes are discussed. Finally, on the basis of the present kinetic data and Scheme 1, the temperature and pressure dependence of the OH radical yield is presented and compared with results reported in previous studies.

3.1. Very Low-Pressure Reactor. Figure 1 shows the relative rate data obtained at 296 K using the Cl + CH_3CHO
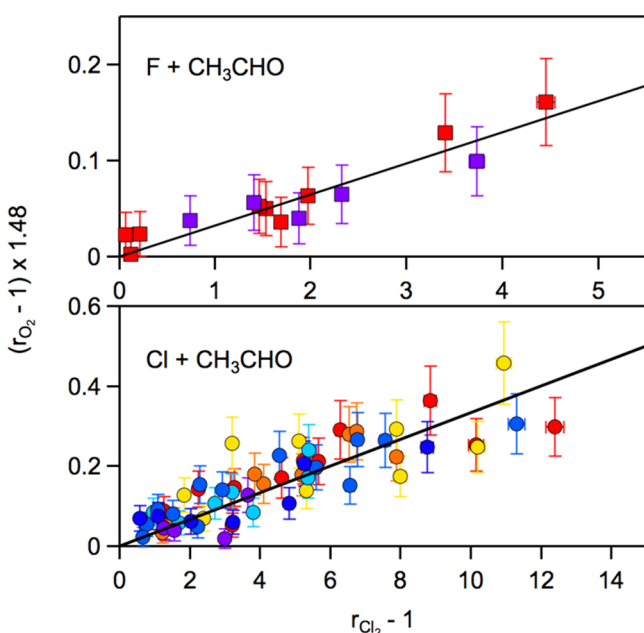
Figure 1. Competitive rate coefficient data for the $CH_3CO + O_2$ reaction obtained in this work at 296 K using the very low-pressure reactor (VLPR) technique with the $CH_3CO + Cl_2$ reaction used as the reference reaction. The upper panel shows the experimental data obtained using the F + CH_3CHO reaction as the CH_3CO radical source and the lower panel shows the results obtained with the Cl + CH_3CHO source chemistry. The error bars on the data points are 2σ of the measurement precision. The different color symbols identify data obtained in independent experiments. The lines are least-squares fits to the combined data for each source (see Table 1) to $((I_0^{O_2}/I_r^{O_2}) - 1)(m_{Cl_2}/m_{O_2})^{1/2} = (k_1/k_{ref})((I_0^{Cl_2}/I_r^{Cl_2}) - 1))$ (eq VII) where r_{Cl_2} and r_{O_2} are the measured quantities $(I_0^{Cl_2}/I_r^{Cl_2})$ and $(I_0^{O_2}/I_r^{O_2})$, respectively, and $(m_{Cl_2}/m_{O_2})^{1/2} = 1.48$.

and F + CH_3CHO reactions as the CH_3CO radical source. Table 1 provides a summary of the experimental conditions and the rate coefficient ratios (k_1/k_{ref}) obtained in the VLPR experiments. The Cl + CH_3CHO source was used for the majority of the experiments with seven independent relative rate measurements performed. The multiple experiments tested the reproducibility of the kinetic results and its sensitivity to a variation in experimental conditions. The measured k_1/k_{ref}

values ranged from 0.024 to 0.038 with measurement precisions of 10 to ~25%. The fairly large scatter in the experimental data is attributed to the large difference between the $CH_3CO + O_2$ and $CH_3CO + Cl_2$ rate coefficients and the discrepancy in the measured changes in the O_2 and Cl_2 concentrations. The greater MS sensitivity for O_2, compared with Cl_2, compensated somewhat for the difference in reaction rate coefficients and made the rate coefficient measurements possible.

Kinetic measurements performed within the 9−32 mTorr pressure range showed no systematic dependence on pressure within the measurement precision and are taken to be representative of the zero-pressure limit bimolecular reaction pathway. The rate coefficient results also showed no measurable dependence on the experimental conditions, that is, variations in the CH_3CHO initial concentration and the Cl_2/O_2 mixing ratio. The rate coefficient determined using the Cl + CH_3CHO radical source was obtained from a fit to all of the data points shown in Figure 1, which yielded $(1.00 \pm 0.08) \times 10^{-12}$ cm^3 molecule^{-1} s^{-1}, where the error limits are from the fit precision. The fit yielded an intercept that was statistically indistinguishable from zero; therefore, the intercept was held to zero in the final analysis. Fits to the individual experiments agreed with this value to within their measurement precision. Several test measurements were also performed using a 2 mm escape orifice, which effectively varies the residence time of reactants in the Knudson reactor. The rate coefficients obtained agreed, to within the measurement precision, with results obtained using the 1 mm escape orifice.

Two complementary measurements were also performed using the F + CH_3CHO reaction as the CH_3CO radical precursor. The experimental data are shown in Figure 1 and summarized in Table 1. As previously described, the F-atom reaction produces both CH_3CO and CH_2CHO radicals; however, analyzing the experimental data using either eq VII (no CH_2CHO radical chemistry) or eq X (including CH_2CHO radical chemistry) yielded similar results for k_1/k_{ref} with the differences being significantly less than the precision of the measurements. In particular, $k_1(296$ K,$M)$ obtained using eq VII was $(9.72 \pm 1.10) \times 10^{-13}$ cm^3 molecule^{-1} s^{-1}, while a value of $(9.88 \pm 1.12) \times 10^{-13}$ cm^3 molecule^{-1} s^{-1} was obtained using eq X with $k_6(296$ K, 10 mTorr$)$ taken to be 5.15×10^{-16} cm^3 molecule^{-1} s^{-1}[33] and an estimated value of 1×10^{-12} cm^3 molecule^{-1} s^{-1} for k_7. The rate coefficient obtained with the F-atom source chemistry was nearly the same as the value obtained using the Cl + CH_3CHO source for CH_3CO radicals. We report a final low-pressure rate coefficient of $(9.94 \pm 1.3) \times 10^{-13}$ cm^3 molecule^{-1} s^{-1}, which is an average of the values obtained using the two CH_3CO radical sources, where the quoted uncertainty includes the full range of the individually measured values.

3.2. Pulsed Laser Photolysis−Laser-Induced Fluorescence. Figure 2 shows representative OH temporal profiles obtained at 296 K and 100 Torr (He) for a range of O_2 concentrations. The quality of the experimental data shown in Figure 2 is representative of the overall quality of the profiles measured under other experimental conditions. The OH temporal profiles are defined by a rapid initial rise following the pulsed laser photolytic production of CH_3CO. The OH signal reaches a maximum value within ~100 μs under the conditions of our experiments with an ensuing slow decay. The pseudo-first order rate coefficient for the OH signal rise was dependent on total pressure and temperature with the measured values in the range $(1.3−60) \times 10^4$ s^{-1}. The first-

Table 1. Summary of Experimental Conditions and Rate Coefficients Obtained for the $CH_3CO + O_2 + M$ (He) Reaction at 296 K Using the Relative Rate Very Low-Pressure Reactor (VLPR) Technique

CH₃CO radical source	pressure range (mTorr)	reactor residence time (s) (X = F or Cl)					$[Cl_2]$ range $(10^{13})^a$	$[O_2]$ range $(10^{14})^a$	$k/k_{ref}{}^b$	$k(296\ K)$ $(10^{-12}\ cm^3\ molecule^{-1}\ s^{-1})^{b,c}$
		X_2	X	O_2	CH_3CHO	CH_3CO				
Cl + CH₃CHO	9–12	9.7	6.9	6.6	7.7	7.6	0.49–5.5	2.0–2.9	0.032 ± 0.006	0.96 ± 0.17
							0.60–5.0	2.1–2.8	0.037 ± 0.005	1.11 ± 0.15
							0.87–5.5	2.1–2.8	0.034 ± 0.009	1.02 ± 0.26
							0.33–3.0	2.1–2.9	0.037 ± 0.008	1.11 ± 0.23
							0.38–3.2	2.0–2.9	0.033 ± 0.005	0.99 ± 0.16
							0.50–4.0	2.0–2.7	0.029 ± 0.007	0.87 ± 0.20
							0.55–4.7	2.1–2.9	0.024 ± 0.014	0.72 ± 0.42
									$0.033 ± 0.003^d$	$1.00 ± 0.08^d$
F + CH₃CHO	20–32	7.2	5.1	6.6	7.7	7.6	0.8–5.4	2.4–2.9	0.038 ± 0.006	1.14 ± 0.11
							1.2–5.5	2.4–2.9	0.028 ± 0.005	0.84 ± 0.17
									$0.033 ± 0.004^d$	$0.99 ± 0.11^d$

[a]Units: molecules cm⁻³. [b]The quoted uncertainties are 2σ (95% confidence interval) of the measurement precision. [c]k_{ref} for the $Cl_2 + CH_3CO$ reference reaction was taken from Gierczak et al.,[32] $(3.0 ± 0.5) \times 10^{-11}$ cm³ molecule⁻¹ s⁻¹. [d]The rate coefficient ratio and $k(296\ K)$ were obtained from a linear least-squares fit of all data obtained using the same radical source.
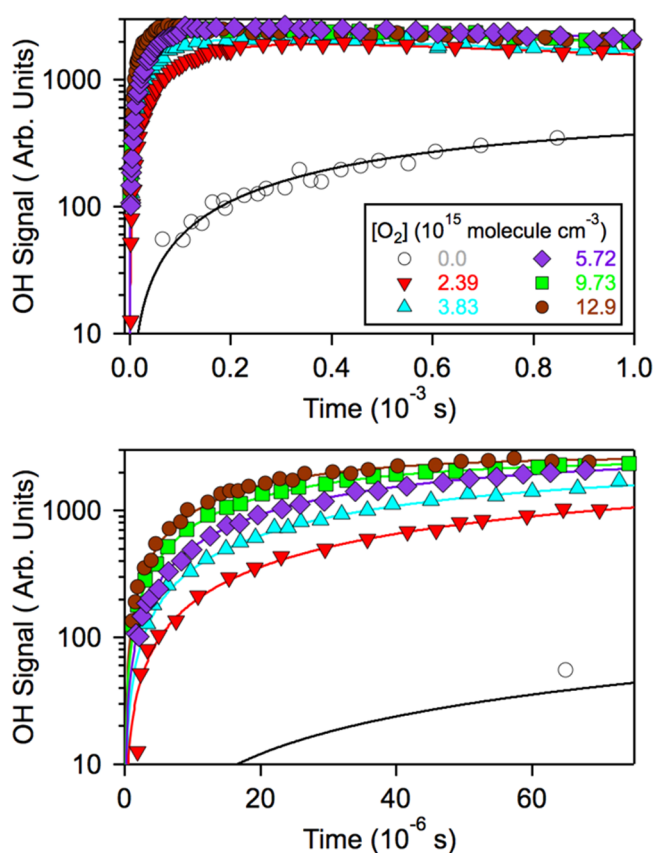
Figure 2. Representative OH temporal profiles recorded at 296 K and 100 Torr (He) total pressure in the pulsed laser photolysis–laser-induced fluorescence (PLP–LIF) experiments. In these experiments, CH₃CO radicals were produced via the 280 nm photolysis of $CH_3C(O)CH_3$. The upper panel shows the profiles over the first 1 ms following the photolysis laser pulse, while the lower panel shows the same experimental data over the first 75 µs. The O₂ concentrations are given in the legend. The lines are nonlinear least-squares fits of the data to eq I. The experimental conditions and kinetic results obtained using the PLP–LIF technique are summarized in Tables 2 and 3

order loss rate coefficients were in the range 100 to 3000 s⁻¹. The first 1500 µs of the OH temporal profile following the

photolysis laser pulse was used in the fit of the experimental data to eq I. The fits are included in Figure 2 and reproduce the experimental data, under all conditions, to within the measurement precision. As shown in Figure 2, a weak OH temporal background signal was observed in the absence of added O₂. An OH background signal was observed in measurements under all experimental conditions and with each of the CH₃CO radical photolytic sources. Experimental tests for the origin of the background signal are discussed in the error analysis section.

Figure 3 summarizes the pseudo-first-order rate coefficient data obtained at 373 K. The $k'(373\ K,M)$ data obtained at total pressures of 20, 50, 100, and 200 Torr (He) showed a linear
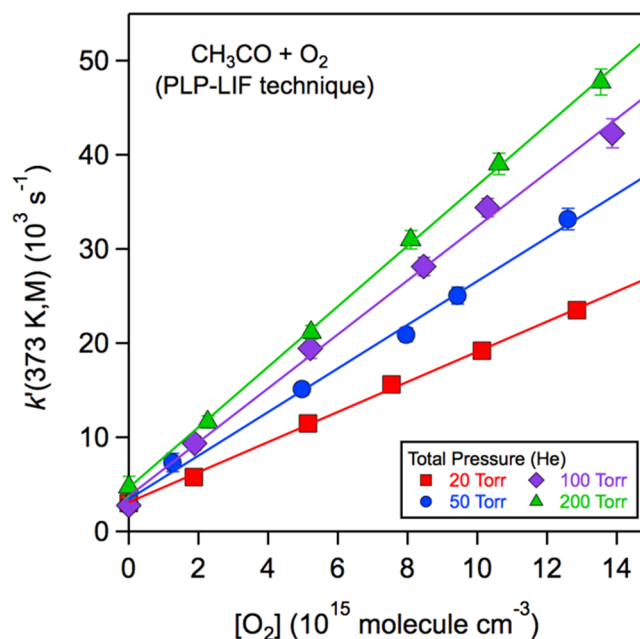

Figure 3. Pseudo-first-order rate coefficient data for the $CH_3CO + O_2$ reaction at 373 K obtained using the pulsed laser photolysis-laser-induced fluorescence (PLP–LIF) technique at the total pressures given in the legend. The lines are linear least-squares fits of the data. A summary of the experimental conditions and kinetic results is given in Tables 2 and 3.

Table 2. Summary of the Experimental Conditions and Rate Coefficients Obtained in This Work for the Gas-Phase CH_3CO + O_2 + M (He) Reaction Using the Pulsed Laser Photolysis–Laser-Induced Fluorescence (PLP–LIF) Technique

T (K)	number density (10^{18} molecules cm^{-3})	CH_3CO radical photolytic source[a]	[O_2] range (10^{15} molecules cm^{-3})	k (10^{-12} cm^3 molecule^{-1} s^{-1})[b]
241	0.39	$CH_3C(O)CH_3$	1.8–10.5	3.35 ± 0.09
	0.78	$CH_3C(O)CH_3$	1.6–12.3	3.91 ± 0.26
	2.04	$CH_3C(O)CH_3$	1.9–12.0	4.68 ± 0.04
	3.98	$CH_3C(O)CH_3$	1.4–10.6	5.20 ± 0.13
	8.04	$CH_3C(O)CH_3$	2.1–13.0	5.21 ± 1.10
296	0.27	$CH_3C(O)CH_3$	2.9–13.6	2.21 ± 0.10
	0.28	$CH_3C(O)CH_3$ (280 nm)	1.5–11.1	1.88 ± 0.22
				2.09 ±0.12[c]
	0.58	$CH_3C(O)CH_3$	2.0–12.9	2.63 ± 0.06
	0.59	$CH_3C(O)CH_3$	2.7–12.6	2.79 ± 0.07
	0.60	$CH_3C(O)CH_3$	1.7–12.5	2.74 ± 0.06
				2.72 ±0.13[c]
	1.15	$CH_3C(O)CH_3$ (280 nm)	2.5–16.7	2.73 ± 0.12
	1.14	$CH_3C(O)CH_3$	2.1–13.0	3.15 ± 0.10
				3.00 ±0.34[c]
	1.63	CH_3CClO	1.8–11.6	3.14 ± 0.11
	1.62	$CH_3C(O)CH_3$	1.7–13.5	3.63 ± 0.16
	1.58	$CH_3C(O)CH_3$ (280 nm)	2.1–13.6	3.08 ± 0.13
				3.36 ±0.47[c]
	2.44	CH_3CClO	2.9–11.7	3.53 ± 0.20
	3.20	$CH_3C(O)CH_3$	1.6–16.1	3.71 ± 0.14
	3.26	$CH_3C(O)CH_3$	1.6–22.5	3.91 ± 0.08
	3.26	CH_3CClO	2.0–12.7	3.86 ± 0.08
	3.26	$CH_3C(O)CH_3$	4.4–12.6	3.77 ± 0.20
	3.26	$CH_3C(O)CH_3$(280 nm)	2.4–15.0	3.74 ± 0.40
	3.26	$CH_3C(O)CH_3$	2.5–12.3	3.87 ± 0.43
				3.80 ±0.29[c]
	6.49	$CH_3C(O)CH_3$	2.1–10.0	4.24 ± 0.33
373	0.27	$CH_3C(O)CH_3$	1.3–7.2	1.18 ± 0.07
	0.52	$CH_3C(O)CH_3$	1.9–12.9	1.60 ± 0.05
	1.28	$CH_3C(O)CH_3$	1.2–12.6	2.26 ± 0.20
	1.99	$CH_3C(O)CH_3$	2.1–12.9	2.47 ± 0.14
	2.59	$CH_3C(O)CH_3$	1.9–13.9	2.78 ± 0.18
	5.18	$CH_3C(O)CH_3$	2.3–13.6	3.21 ± 0.07

[a]248 nm pulsed laser photolysis unless noted otherwise. [b]Quoted uncertainties are 2σ (95% confidence interval) of the measurement precision. [c]Rate coefficient was obtained from a linear least-squares fit of all data obtained at the same temperature and pressure.

dependence on the O_2 concentration. The data also clearly show an increase in k'(373 K,M) with increasing total pressure consistent with Scheme 1. Linear least-squares fits, included in Figure 3, reproduce the experimental data very well, and the slope yields the rate coefficient at each pressure. The fits also yielded a substantial intercept at zero O_2 concentration, that is, a CH_3CO loss in the absence of added O_2. The intercept is roughly consistent with the rate coefficient for the rise in the background OH signal, for example, as illustrated in Figure 2. A significant intercept was observed at all temperatures included in this study and is discussed further in the Error Analysis section.

A summary of the experimental conditions and the phenomenological rate coefficients obtained for the gas-phase CH_3CO + O_2 reaction is given in Tables 2 and 3 for He and N_2 bath gases, respectively. The kinetic measurements obtained using two different CH_3CO radical sources, different initial radical concentrations, and other variations in experimental conditions as outlined in the Tables were consistent to within the measurement precision. The rate coefficients obtained show a systematic dependence on the total number density that is more apparent at the higher temperatures. A negative

temperature dependence in the rate coefficient data was also observed at all pressures. This behavior is consistent with the reaction mechanism given in Scheme 1. Figure 4 shows the second-order rate coefficient data obtained using the PLP–LIF method over a range of pressure (number density) at 241, 296, and 373 K for N_2 and He bath gases. The experimental data show falloff behavior over the pressure range included in this study, 10 to 200 Torr, and a systematic dependence on the bath gas, that is, energy-transfer collision efficiency.

3.3. Pulsed Laser Photolysis-Cavity Ring-down Spectroscopy (PLP–CRDS). Figure 5 shows a representative set of CRDS SKaR profiles obtained in this work at 295 K and 100 Torr (He). SKaR profiles obtained under other experimental conditions were of similar quality to those shown in Figure 5. SKaR profiles were measured at each pressure with a variation in the O_2 concentration of a factor of ~10. The experimental data were reproduced to within the measurement precision by a fit to eq III from which pseudo-first-order rate coefficients were obtained. A second-order kinetic data plot is also included in Figure 5. k' varied linearly with [O_2], and a linear least-squares fit of k' versus [O_2] yielded k_1(295 K,M). A summary of the

Table 3. Summary of the Experimental Conditions and Rate Coefficients Obtained in This Work for the Gas-Phase CH$_3$CO + O$_2$ + M (N$_2$) Reaction Using the Pulsed Laser Photolysis–Laser-Induced Fluorescence (PLP–LIF) Technique

T (K)	number density (10^{18} molecules cm^{-3})	CH$_3$CO radical photolysis source[a]	[O$_2$] range (10^{15} molecules cm^{-3})	k (10^{-12} cm^3 molecule^{-1} s^{-1})[b]
241	0.41	CH$_3$C(O)CH$_3$	1.7–11.7	3.61 ± 0.10
	0.79	CH$_3$C(O)CH$_3$	1.8–12.9	4.27 ± 0.12
	2.01	CH$_3$C(O)CH$_3$	2.1–13.3	4.96 ± 0.06
	3.95	CH$_3$C(O)CH$_3$	2.9–16.9	5.43 ± 0.60
296	0.28	CH$_3$C(O)CH$_3$	1.7–10.5	2.46 ± 0.07
	0.58	CH$_3$C(O)CH$_3$	2.0–11.6	2.92 ± 0.12
	1.13	CH$_3$C(O)CH$_3$	2.2–13.3	3.46 ± 0.12
	1.15	CH$_3$C(O)CH$_3$ (280 nm)	2.0–12.6	3.18 ± 0.20
				3.36 ± 0.19[c]
	1.58	CH$_3$C(O)CH$_3$	2.5–13.5	3.83 ± 0.09
	1.62	CH$_3$C(O)CH$_3$ (280 nm)	1.7–11.1	3.73 ± 0.12
				3.78 ± 0.08[c]
	2.46	CH$_3$C(O)CH$_3$	2.7–12.1	3.95 ± 0.41
	3.26	CH$_3$C(O)CH$_3$ (280 nm)	1.4–11.4	4.25 ± 0.20
	3.26	CH$_3$CClO	2.8–25.4	3.99 ± 0.08
	3.26	CH$_3$CClO	2.6–21.6	4.08 ± 0.31
	3.26	CH$_3$C(O)CH$_3$	2.1–29.0	4.19 ± 0.28
	3.28	CH$_3$C(O)CH$_3$	2.0–12.6	4.33 ± 0.72
				4.28 ± 0.24[c]
	6.48	CH$_3$C(O)CH$_3$	2.6–12.4	4.38 ± 0.41
373	0.26	CH$_3$C(O)CH$_3$	1.5–11.6	1.44 ± 0.15
	0.52	CH$_3$C(O)CH$_3$	1.1–11.7	1.94 ± 0.08
	1.28	CH$_3$C(O)CH$_3$	1.6–12.3	2.42 ± 0.06
	1.99	CH$_3$C(O)CH$_3$	1.8–11.8	3.00 ± 0.16
	2.58	CH$_3$C(O)CH$_3$	1.8–12.1	3.21 ± 0.07
	5.62	CH$_3$C(O)CH$_3$	3.5–14.5	3.49 ± 0.40

[a]248 nm pulsed laser photolysis unless noted otherwise. [b]Quoted uncertainties are 2σ (95% confidence interval) of the measurement precision. [c]Rate coefficient was obtained from a linear least-squares fit of all data obtained at the same temperature and pressure.

experimental conditions and rate coefficients obtained at total pressures between 25 and 600 Torr (He) is given in Table 4.

The first-order loss of CH$_3$CO in the absence of added O$_2$ included in Figure 5 was measured using a time delay approach because the CH$_3$CO loss was too slow compared with the ring-down time constant to effectively use the SKaR technique. Typical values of k' in the absence of O$_2$ were in the range 400 to 1800 s^{-1} with no apparent dependence on the radical concentration or total pressure. The observed k' in the absence of added O$_2$ is greater than that due solely to diffusive losses from the reactor reaction volume and, most likely, represents an unidentified reactive loss. The observation of a statistically significant background CH$_3$CO radical loss process is consistent with the observations in the PLP–LIF experiments previously described.

The $k_1(T,M)$ data obtained using the PLP–CRDS method are included in Figure 4. The kinetic results obtained in the CRDS experiments show slightly greater scatter than the PLP–LIF data, but overall are in good agreement with the PLP–LIF results.

3.4. Error Analysis. The absolute accuracy of the rate coefficients reported in this work was determined by the precision of the experimental measurements, potential systematic errors associated with the measurements and data analysis, and the level of agreement between measurements performed under similar conditions using different kinetic methods. The three experimental methods had different potential systematic errors associated with them, which were evaluated experimentally by performing measurements over a range of conditions. The uncertainties associated with the three experimental techniques employed in this study are considered separately.

The uncertainty associated with the data obtained in the VLPR experiments depended on the accuracy of the measured change in both the O$_2$ and Cl$_2$ concentrations. The uncertainties included in Figure 1 are the propagated errors in the $((I_0^{Cl_2}/I_r^{Cl_2}) - 1)$ and $1.48((I_0^{O_2}/I_r^{O_2}) - 1)$ expressions with a ΔI uncertainty of 2% for the Cl$_2$ intensity measurement and 4% for the O$_2$ measurement over the entire range of intensities measured for each species. The uncertainty in the individual data points was typically in the range 20 to 30% for the O$_2$ ratio measurements and ~10% for the Cl$_2$ measurements; see Figure 1. The measurement uncertainty was, in part, due to the large difference between k_1(296 K,M) and the reference reaction rate coefficient. A CH$_3$CO reference reaction with a rate coefficient similar to k_1(296 K,M) would have been preferred but is not available. The fit precisions of the individual k/k_{ref} determinations were ~10%; see Table 1. Different CH$_3$CO source chemistry and experimental conditions (see Table 1) were employed to test the precision and the reliability of the kinetic measurements. The k/k_{ref} results obtained in nine independent experiments agreed to within ~25%, while the average k/k_{ref} values obtained using the different radical sources were nearly identical with an uncertainty of ~10%. Another significant source of potential systematic error in the VLPR k_1(296 K,M) determination is the uncertainty in the reference reaction rate coefficient, which for the CH$_3$CO + Cl$_2$ reaction was estimated to be 17%.[32] We estimate the absolute uncertainty in k_1(296 K,M) measured using the VLPR method to be ~20%.
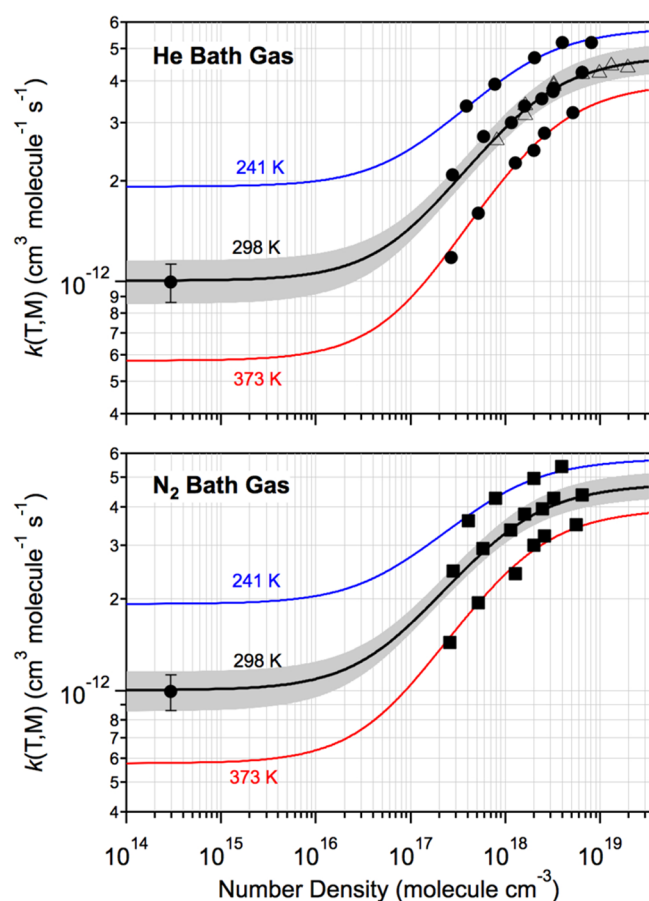
Figure 4. Rate coefficient data for the $CH_3CO + O_2$ reaction obtained in this work at 241, 296, and 373 K and pressures over the range 0.009 to 600 Torr for He and N_2 bath gases. Kinetic data were obtained using the pulsed laser photolysis–laser-induced fluorescence (PLP–LIF) (circles and squares at number densities greater than 2×10^{17} molecules cm^{-3}), PLP–cavity ring-down spectroscopy (PLP–CRDS) (triangles), and a very low-pressure reactor (VLPR) (circles with error bar) techniques (see text). A summary of the experimental conditions and kinetic data is given in Tables 1–4. Error bars on the high-pressure data are not included for clarity but are given in the Tables. The lines are least-squares fits of the data with $F_c = 0.8$. The fit results are summarized in Table 5. The gray shading represents the estimated 2σ uncertainty range in the 298 K fit.

Figure 5. Representative cavity ring-down spectroscopy (CRDS) kinetic data for the $CH_3CO + O_2$ reaction obtained at 295 K and 100 Torr (He) with pulsed laser photolysis of acetone as the CH_3CO radical source. (See Table 4.) Top panel: SKaR temporal profiles (see the text) measured with different O_2 concentrations (increasing O_2 concentration from top to bottom). The lines are least-squares fits of the data to eq III. Bottom panel: Pseudo-first-order rate coefficient data obtained from the profiles given in the top panel (color-coded). The data point in gray (second greatest k') is not shown in the top panel for clarity. The SKaR method was not used to obtain the slow decay at $[O_2] = 0$; it was obtained by monitoring the CH_3CO radical decay over longer reaction times. The line is a linear least-squares fit of the data.

The measurement precision in the PLP–LIF experiments was high with deviations of <6%; see Tables 2 and 3 and Figure 3. The overall quality of the data, as shown in Figure 2, illustrates the high degree of repeatability and reproducibility obtained in the OH temporal profile measurements. Typically, ~30 data points were collected over the rise portion of the OH profile. The high stability and precision of the OH temporal profile measurements enabled precise fits of the data to eq I. The analysis reproduced the experimental data to within the measurement precision over the entire measurement time scale. The O_2 concentration was measured using gas flow rates with an estimated uncertainty of <5%. Uncertainties in the O_2 concentration due to the uncertainty in the reactor temperature and pressure were minor, <2%, and we estimate an overall uncertainty in $[O_2]$ to be <6%. Variation of photolysis laser fluence, initial radical concentration, CH_3CO radical source, linear flow velocity and other experimental conditions had a negligible effect in the measured rate coefficients. We estimate the absolute uncertainty in $k_1(T,M)$ measured using the PLP–
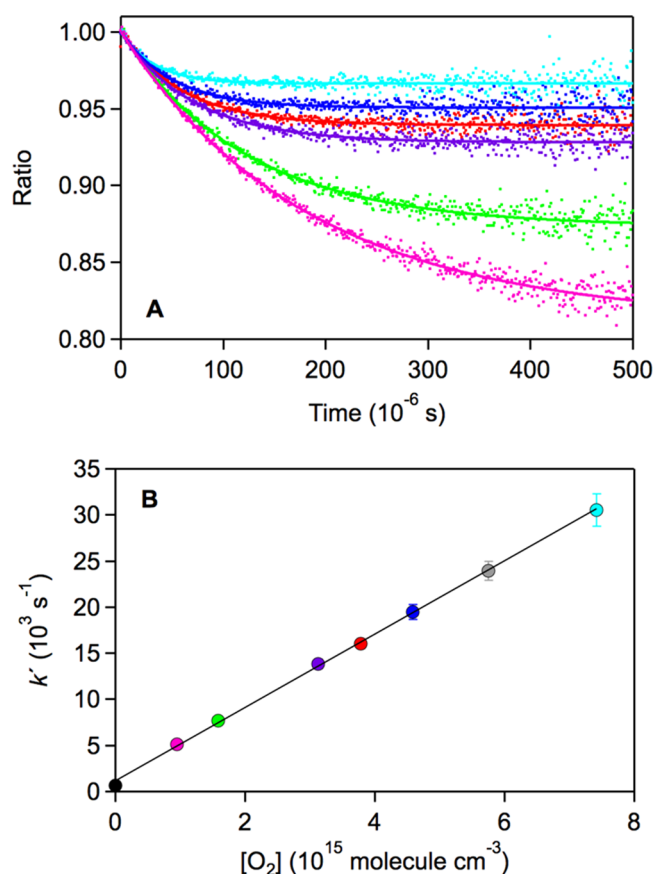
LIF method to be 8% for all temperatures and pressures included in this study.

A weak temporal OH signal was observed in all PLP–LIF experiments made in the absence of added O_2 (e.g., see Figure 2). The magnitude of the OH signal did not significantly impact the determination of $k_1(T,M)$, but several test experiments were performed in an attempt to identify its origin. First, OH temporal profiles were measured at 100 Torr and 296 K with low concentrations of O_2 added to the system, $(0.5-50) \times 10^{14}$ molecules cm^{-3}, to evaluate the contribution from potential O_2 impurities. The addition of O_2 within this range did not substantially affect either the absolute magnitude or the rate of rise of the observed background OH signal. Therefore, system leaks of O_2 are unlikely to account for the observed OH signal in the absence of O_2 addition. Experiments were also performed at 296 K and 10 and 200 Torr total pressure without O_2 added to the system. The background OH signal and the rate of rise was not significantly different over this range of pressure, which suggests that it was not due to an O_2 impurity in the bath gas.

Table 4. Summary of Experimental Conditions and Rate Coefficients Obtained for the Gas-Phase CH$_3$CO + O$_2$ + M (He) Reaction at 295 K Using the Cavity Ring-Down Spectroscopy (CRDS) Technique

pressure (Torr, He)	[CH$_3$CO]$_0$ range (10^{12} molecules cm^{-3})^a	[O$_2$] range (10^{15} molecules cm^{-3})	k' range (s^{-1})	k_1(295 K) (10^{-12} cm^3 molecule^{-1} s^{-1})^b
600	4.7–6.6	1.18–7.04	7065–32520	4.38 ± 0.20
400	4.7–5.9	0.68–7.11	4300–31950	4.44 ± 0.16
300	4.1–5.4	0.91–11.3	4930–48250	4.22 ± 0.16
200	6.5–6.9	0.95–7.42	5160–30540	4.18 ± 0.08
100	5.9–7.2^c	0.76–7.43	3855–27170	3.85 ± 0.06
100	5.1–5.8	0.48–6.66	3750–25250	3.90 ± 0.07
50	3.3–3.6	0.76–7.35	3200–18650	3.15 ± 0.08
50	3.3–3.6	1.15–7.77	3066–26850	3.37 ± 0.05
25	5.0–5.6	0.75–7.37	3200–20950	2.64 ± 0.05

^{a}248 nm pulsed laser photolysis of acetone (CH$_3$C(O)CH$_3$) was used as the CH$_3$CO radical source unless noted otherwise. ^{b}Quoted uncertainties are 2σ (95% confidence interval) of the measurement precision. ^{c}The acetyl radical was produced via the 248 nm pulsed laser photolysis of acetyl chloride (CH$_3$CClO).

OH radical production in the CH$_3$ + O$_2$ reaction, which is analogous to reaction 1,

$$CH_3 + O_2 \rightarrow OH + \text{products} \tag{6a}$$

$$CH_3 + O_2 + M \rightarrow CH_3O_2 \tag{6b}$$
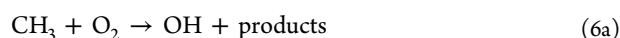
was also tested. CH$_3$ radicals are produced as a primary photolysis coproduct in the CH$_3$CO radical sources used in this study. The kinetics of reaction 6 have been extensively studied, and the recommended rate coefficients for the bimolecular (6a) and termolecular (6b) channels are $k_{6a} < 3 \times 10^{-16}$ cm^3 molecule^{-1} s^{-1} and $k_0(T) = 4 \times 10^{-31}(T/300)^{-3.6}$ cm^6 molecule^{-2} s^{-1} and $k_\infty(T) = 1.2 \times 10^{-12}(T/300)^{1.1}$ cm^3 molecule^{-1} s^{-1}.[2] Therefore, the OH yield in reaction 6 is expected to be small under the conditions of our experiments, <0.001 at 20 Torr total pressure. To isolate the CH$_3$ radical chemistry, we performed an experiment using the 248 nm pulsed laser photolysis of CH$_3$I (CH$_3$I + $h\nu$ → CH$_3$ + I) at 296 K and 100 Torr (He). The CH$_3$I concentration was ~10^{15} molecules cm^{-3} and the O$_2$ concentration was ~8 × 10^{15} molecules cm^{-3}. The initial CH$_3$ radical concentration was estimated to be ~1 × 10^{13} radicals cm^{-3}, which is much greater than the radical concentrations used in our kinetic measurements of reaction 1. On the basis of this single measurement, the rate coefficient for the reaction of CH$_3$ radicals with O$_2$ was <5 × 10^{-13} cm^3 molecule^{-1} s^{-1}, which is consistent with its recommended value.[2] Reaction 6 would therefore contribute <10% to the observed weak background OH signal.

In addition, over the course of our study, two different photolysis wavelengths (248 and 280 nm) as well as two different CH$_3$CO precursors were used. The different photolysis sources and wavelengths lead to significantly different CH$_3$ radical yields as well as the ratio of the initial CH$_3$CO and CH$_3$ radical concentrations. No substantial difference in the OH background signal was observed, which also suggests that reaction 6 makes only a minor contribution to the observed total OH background signal. We estimate that this pathway contributes <2% to the total background OH signal under the range of conditions used in this study. The results of our test measurements imply that the background OH signal is not due to reaction 1. The origin of the background OH signal and the CH$_3$CO radical loss in the absence of added O$_2$ observed in our PLP–LIF and PLP–CRDS experiments is presently unknown but may involve as yet unidentified excited- or ground-state chemistry of the CH$_3$CO radical. The background OH signal and CH$_3$CO radical loss in the absence of added O$_2$, however, had a negligible impact on our kinetic measurements for reaction 1 and the evaluation of the OH radical yield described later.

The precision of the PLP–CRDS kinetic measurements was high. The CH$_3$CO ring-down profile ratios were obtained over a range of CH$_3$CO and O$_2$ concentrations, and the fits to eq III (see Figure 5) reproduced the experimental data to within the measurement precision. The second-order kinetic plot (Figure 5) shows a linear dependence on the O$_2$ concentration with linear least-squares fit precisions better than 5% (See Table 4). Kinetic measurements performed at 100 Torr (He) using 248 nm pulsed laser photolysis of CH$_3$C(O)CH$_3$ and CH$_3$CClO as the CH$_3$CO radical source agreed to well within their measurement precisions. We estimate the k_1(295 K,M) values measured using the PLP–CRDS technique to have an absolute uncertainty of ~10%. The k_1(295 K, M) values obtained over the pressure range 25 to 600 Torr showed a falloff behavior that is in agreement with the PLP–LIF kinetic results obtained over the pressure range ~10 to 200 Torr (He).

4. REACTION FALL-OFF BEHAVIOR

The rate coefficient data obtained in this study (Tables 1–4) is plotted in Figure 4. Over the pressure range included in the present study, 0.009 to 600 Torr, the phenomenological rate coefficient, $k_1(T,M)$, exhibits a combination of bimolecular and termolecular behavior consistent with the reaction mechanism given in Scheme 1, where $k_1(T,M)$ is the sum of the OH yield channel (bimolecular, k_{bi}) and CH$_3$C(O)O$_2$ yield channel (termolecular, k_{ter}) rate coefficients

$$k_1(T, M) = k_{bi}(T, M) + k_{ter}(T, M) \tag{XI}$$

The formulas that describe the falloff behavior as given in Tyndall et al.[11] for $k_{bi}(T,M)$ and $k_{ter}(T,M)$ are reproduced here

$$k_{ter}(T, M) = \left(\frac{k_\infty(T)k_0(T)[M]}{k_0(T)[M] + k_\infty(T)} \right) F_C^\gamma \tag{XII}$$

$$k_{bi}(T, M) = k_{int}\left(1 - \frac{k_0(T)[M]F_C^\gamma}{k_0(T)[M] + k_\infty(T)} \right) \tag{XIII}$$

where

$$k_\infty(T) = k_1 \tag{XIV}$$

$$k_0(T) = \frac{k_1 k_3}{k_{-1} + k_2} \tag{XV}$$

Table 5. Fall-off Behavior Fit Results for the CH$_3$CO + O$_2$ Reaction and the Sensitivity to F_c

	fit value[a]		
parameter	$F_c = 0.6$	$F_c = 0.8$	$F_c = 0.95$
$k_0(300\ \mathrm{K})$[b]	$(12.9 \pm 0.07) \times 10^{-30}$	$(7.39 \pm 0.34) \times 10^{-30}$	$(5.28 \pm 0.2) \times 10^{-30}$
n	(2.2 ± 0.3)	(2.2 ± 0.3)	(2.1 ± 0.2)
$k_\infty(300\ \mathrm{K})$[c]	$(5.11 \pm 0.06) \times 10^{-12}$	$(4.88 \pm 0.05) \times 10^{-12}$	$(4.67 \pm 0.05) \times 10^{-12}$
m	(0.8 ± 0.08)	(0.85 ± 0.07)	(0.90 ± 0.07)
$\beta(\mathrm{N}_2)$	1	1	1
$\beta(\mathrm{He})$	(0.59 ± 0.05)	(0.60 ± 0.05)	(0.60 ± 0.05)
$k_{int}(298\ \mathrm{K})$[c]	9.64×10^{-13}	10.2×10^{-13}	11.0×10^{-13}
A[c]	$(5.1 \pm 3) \times 10^{-14}$	$(6.4 \pm 4) \times 10^{-14}$	$(7.9 \pm 4) \times 10^{-14}$
E/R (K)	(-870 ± 145)	(-820 ± 150)	(-780 ± 145)

[a]Values were determined from a nonlinear least-squares fit of all the experimental data obtained in this work, see Tables 1−4. The quoted uncertainties are 1σ from the fit precision. The $k_0(300\ \mathrm{K})$ and $k_\infty(300\ \mathrm{K})$ values were obtained from the fit with all other parameters fixed to the rounded-off values given in the Table. $\beta(\mathrm{N}_2)$ was defined to be 1. [b]Units: cm^6 molecule^{-2} s^{-1}. [c]Units: cm^3 molecule^{-1} s^{-1}.

$$k_{int}(T) = \frac{k_1 k_2}{k_{-1} + k_2} \tag{XVI}$$

$$\gamma = \left\{ 1 + \left[\log_{10}\left(\frac{k_0(T)[\mathrm{M}]}{k_\infty(T)} \right) \right]^2 \right\}^{-1} \tag{XVII}$$

and

$$k_0(T) = k_0(300\ \mathrm{K}) \times \left(\frac{T}{300} \right)^{-n} \tag{XVIII}$$

$$k_\infty(T) = k_\infty(300\ \mathrm{K}) \times \left(\frac{T}{300} \right)^{-m} \tag{XIX}$$

The OH radical yield, $Y(T,M)$, for reaction 1 is

$$Y(T, M) = \frac{k_{bi}(T, M)}{k_{bi}(T, M) + k_{ter}(T, M)} \tag{XX}$$

It is important to note that $k_{bi}(T)$ equals $k_{int}(T)$ in the low-pressure limit and approaches zero asymptotically at high pressure. $k_0(300\ \mathrm{K})$, $k_\infty(300\ \mathrm{K})$, n, m, and F_c are parameters that were determined in a fit of the $k_1(T,M)$ data. $k_{int}(T)$ is also a parameter in the fit, while our low-pressure VLPR rate coefficient defines $k_{int}(296\ \mathrm{K})$. The temperature dependence of $k_{int}(T)$ is described by an Arrhenius expression, $k_{int}(T) = A \exp(E/RT)$, where A and E are fit parameters.

The results of a global nonlinear least-squares fit of the experimental data to eq XI are given in Table 5. The optimized value of the F_c parameter was determined to be 0.80 ± 0.12. The fit results presented in Table 5 were obtained with F_c fixed to values of 0.6, 0.8, and 0.95, which are the values of F_c used in the NASA/JPL recommendations for termolecular reactions, our optimized value, and the value used in the Carr et al.[7] study, respectively. All three F_c values reproduce the experimental data well, although with different sets of fit parameters. The final fits were performed with $k_{int}(296\ \mathrm{K})$ fixed to the experimental value obtained in this work but with the Arrhenius A and E parameters allowed to vary. The fit results obtained with $F_c = 0.8$ are included in Figure 4 and reproduce the experimental data obtained with both bath gases very well over the entire range of pressures and temperatures included in this work.

$k_{int}(T)$ was found to have a negative temperature dependence, $E/R = (-820 \pm 150)$ K, which is consistent with a radical reaction proceeding through an intermediate adduct. The parameters describing the termolecular reaction channel exhibit

some degree of correlation; therefore, the parameters derived from the fit do not represent a unique solution. A limitation, for example, is in the determination of $k_\infty(T)$, the high-pressure limit for reaction 1, which was based on experimental data that did not reach the high-pressure limit under the range of our experimental conditions. In addition, there is a strong dependence of the values determined for $k_\infty(300\ \mathrm{K})$ and $k_0(300\ \mathrm{K})$ on the value of F_c. Therefore, although the termolecular reaction channel parameters obtained are reasonable in comparison with other reaction systems (see Sander et al.[2]), the combination of parameters is, most likely, better defined than the individual values. The shaded region included in Figure 4 represents the range in the fitted $k_1(296\ \mathrm{K}, M)$ estimated based on a 15% uncertainty in $k_{int}(296\ \mathrm{K})$ and a 10% uncertainty in the higher pressure kinetic data. The range of kinetic uncertainty, particularly in the low-pressure regime, directly impacts the interpretation of the OH radical yield temperature and pressure dependence that is described later.

4.1. OH Radical Yield. The kinetic analysis and rate coefficient parameters previously presented were used to predict the OH radical yield temperature and pressure dependence given by eq XX. The obtained OH yield is displayed in Figures 6 and 7, where the yield for the He bath gas is greater than that for the N$_2$ bath gas due to its less efficient collisional quenching of the CH$_3$C(O)OO* activated complex. At 1 atm total pressure, the calculated room-temperature OH yield is small (∼1%) but not zero. The OH yield increases with decreasing pressure with a value of ∼0.8 at 1 Torr (He). The yield increases further at even lower pressures, although more slowly, as it asymptotically approaches a value of unity in the zero-pressure limit, as defined by Scheme 1. The shaded region included in Figure 6 illustrates the possible range of OH yield values due to the kinetic data uncertainty previously described and shown in Figure 4. As defined by Scheme 1, the absolute uncertainty in the OH yield in the low- and high-pressure regimes is small. At intermediate pressures, where both the bimolecular and termolecular reaction channels contribute to the observed rate coefficient, the uncertainty in the OH yield is the greatest. An uncertainty of ∼10% in the OH yield was obtained for 10 Torr (He).

The kinetic data obtained at 241 and 373 K were used to predict the temperature dependence of the OH radical yield, and the results are also included in Figure 6. The OH yield profiles exhibit a similar pressure dependence to the room-temperature profile. A weak temperature dependence of the
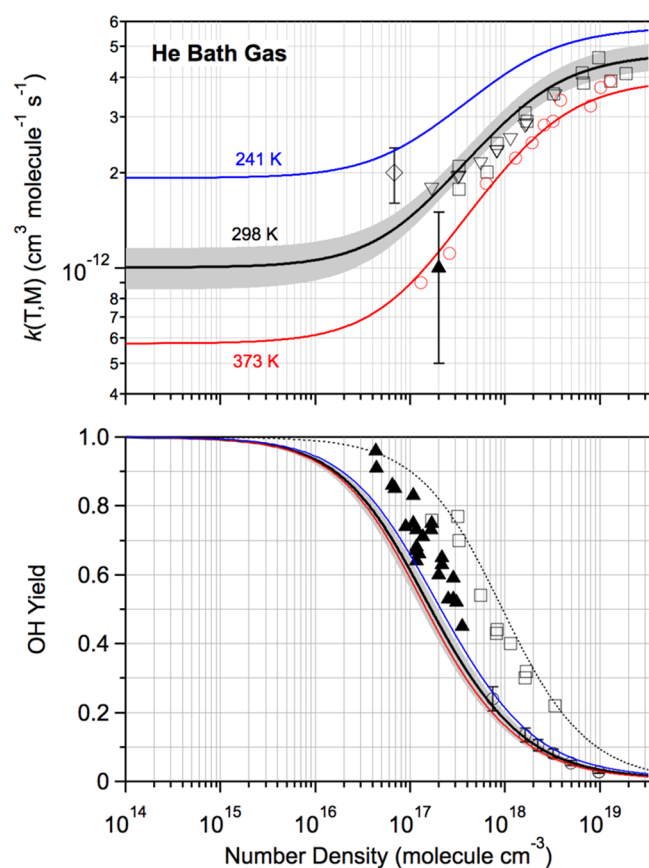
Figure 6. Comparison of $k_1(T,M)$ and OH yield literature data with He bath gas with the results obtained in the present study. Upper panel: $k_1(T,M)$ from this work (solid lines and shaded region (see text)) from Figure 4: Carr et al.[34] at 298 K (inverted triangles); Carr et al.[7] at 298 (squares) and 378 K (red circles); McDade et al. (diamond) at 298 K; and Kovács et al.[8] at 298 K (triangles). Lower panel: The solid black line is the OH yield at 298 K obtained in this work. The gray shaded region represents its estimated uncertainty range based on the uncertainty in the kinetic data shown in the upper panel. (See the text for error analysis.) The blue and red lines are the OH yields at 241 and 373 K, respectively, obtained from the falloff curves shown in the upper panel. The estimated uncertainties at these temperatures are of similar magnitude to the 298 K uncertainty range and are not included for improved clarity: Carr et al.[34] (squares); Carr et al.[7] (dotted line); Groß et al.[35] (circles); and Kovács et al.[8] (triangles).

Figure 7. Comparison of $k_1(T,M)$ and OH yield literature data with N_2 bath gas with the results obtained in the present study. Upper panel: $k_1(T,M)$ from this work (solid lines and shaded region (see text)) from Figure 4: Carr et al.[7] at 298 K (squares) and 378 K (circles); Sehested et al.[10] (SF_6 bath gas, triangle); Kaiser and Wallington[36] (inverted triangle); and Tyndall et al.[11] (dashed line) (scaled to $CH_3CO + Cl_2$ rate coefficient reported in Gierczak et al.[32]). Lower panel: The solid black line is the OH yield at 298 K obtained in this work. The gray shaded region represents its estimated uncertainty range based on the uncertainty in the kinetic data shown in the upper panel. (See the text for error analysis.) The blue and red lines are the OH yields at 241 and 373 K, respectively, obtained from the falloff curves shown in the upper panel. The estimated uncertainties at these temperatures are of similar magnitude to the 298 K uncertainty range and are not included for improved clarity: Carr et al.[34] (squares); Carr et al.[7] (dotted line); Groß et al.[35] (circles); and Tyndall et al.[11] (dashed line, see Table 6).

OH yield was obtained from the nonlinear least-squares fit of our kinetic data with an increase in the OH yield with decreasing temperature. The calculated OH yield temperature dependence is, however, highly correlated with the fitted temperature dependence of $k_{int}(T)$ and therefore is much less certain than the room-temperature OH yield. For $E/R = -820$ K, the optimized fit result, there is a weak negative OH yield temperature dependence, while a value of -600 K, which falls within our uncertainty limits, would lead to the opposite OH yield temperature dependence; for example, the OH yield would increase from 0.34 to 0.38 between 241 and 373 K for 10 Torr He. Therefore, the present kinetic analysis predicts a weak OH yield temperature dependence but cannot clearly determine the trend with temperature. Temperature-dependent rate coefficient data in the low-pressure limit are needed to refine the present analysis.
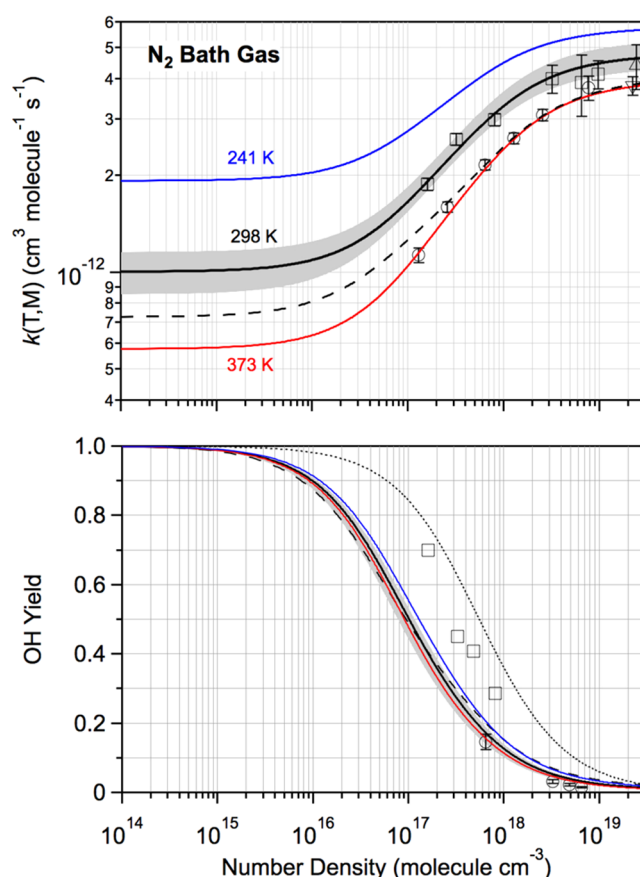
5. COMPARISON WITH PREVIOUS STUDIES OF $k_1(T,M)$ AND $Y(T,M)$

The present $k_1(T,M)$ and $Y(T,M)$ results can be compared directly with several experimental studies available in the literature. Previous studies include measurements made using different experimental techniques applied over a range of temperatures from 213 to 500 K and pressures from 0.1 to 1000 Torr (He, N_2). A summary of the previous $k_1(T,M)$ studies is given in Table 6, and a comparison of the $k_1(T,M)$ and $Y(T,M)$ results with the present work is described later.

The majority of the literature rate coefficient studies were performed at room temperature, and the $k_1(298$ K$,M)$ results are included in Figures 6 and 7 for comparison with the falloff parametrization obtained in our data analysis. Measurements of $k_1(298$ K$,M)$ in the low-pressure regime have been reported by McDade et al.[9] (1−4 Torr, He), Tyndall et al.[11] (>0.1 Torr,

Table 6. Summary of Experimental Conditions and CH$_3$CO + O$_2$ Reaction Rate Coefficient Data Reported in This Work and the Literature

pressure (Torr)	bath gas	temperature (K)	$k_{int}(T)^a$	$k_0(300\ K)/n^b$	$k_\infty(300\ K)/m^a$	F_c	experimental method	reference
0.009–600	He/	241, 296, 373	0.994 ± 0.13	7.82 ± 0.3/	4.87 ± 0.04/	0.8	PLP−LIF/	This study
10–200	N$_2$			2.5 ± 0.5	0.85 ± 0.07		CRDS/VLPR	
1–4	He	298	2.0 ± 0.4				LP−PIMS	McDade et al. (1982)[9]
700	N$_2$	298			3.8 ± 0.25^c		RR	Kaiser and Wallington (1995)[36]
0.1–1100	N$_2$	228, 298	0.73^d	12.3^d	4.3^d	0.6	RR	Tyndall et al. (1997)[11]
750	SF$_6$	295			4.4 ± 0.7		PR/UV−vis	Sehested et al. (1998)[10]
10–400	He	213, 295		4.35 ± 1.49/ 2.49 ± 0.61	6.85 ± 0.81/ 5.17 ± 0.45		LFP−LIF	Blitz et al. (2002)[5]
1–10	He	298	1.0 + 1/−0.5				DF−LIF/RF	Kovács et al. (2007)[8]
	He	213, 296, 378, 500	1.47 ± 0.05	1.64/1.9	6.08/0.02	exp(−T/5600)		Carr et al. (2011)[7]
	N$_2$	298, 378	1.44 ± 0.06	3.64/1.89	6.11/0.01	exp(−T/4600)		

^{a}Units of 10^{-12} cm^3 molecule^{-1} s^{-1}. ^{b}Units of 10^{-30} cm^6 molecule^{-2} s^{-1}. ^{c}Measured rate coefficient ratio, relative to the CH$_3$CO + Cl$_2$ reaction, of 0.126 ± 0.008 (precision) at 700 Torr N$_2$. The rate coefficient given in the Table was obtained using the CH$_3$CO + Cl$_2$ rate coefficient reported in Gierczak et al.[32] ^{d}Corrected fit parameters from those reported in Tyndall et al.[11] (J. Orlando, private communication) scaled (a factor of 1.255 increase) using the CH$_3$CO + Cl$_2$ rate coefficient reported in Gierczak et al.[32] PR/UV−vis: pulsed radiolysis/ultraviolet−visible spectroscopy; PLP−LIF: pulsed laser photolysis-laser-induced fluorescence; RR: relative rate; LFP−LIF: laser flash photolysis−laser-induced fluorescence; DF−LIF/RF: Discharge Flow−Laser-Induced Fluorescence or Resonance Fluorescence

N$_2$), and Kovács et al.[8] (1−10 Torr, He). McDade et al.[9] used a discharge flow−photoionization mass spectrometry technique to monitor CH$_3$CO radical loss following its production in the OH + CH$_3$CHO reaction in the presence of excess O$_2$. Kovács et al.[8] also used a discharge flow method with the same CH$_3$CO radical source chemistry but with LIF and RF detection of the OH radical formed in reaction 1 to determine k_1(298 K,M). Both studies observed no measurable pressure dependence in k_1(298 K,M) over the range of pressures included in their studies. This observation is contrary to the present work that would predict significant changes in k_1(298 K,M) over the 1−4 and 1−10 Torr (He) pressure range with increases of ∼34 and ∼80%, respectively. The calculated increase in k_1(298 K,M), while significant, however, falls within the range of estimated uncertainties in the McDade et al. and Kovács et al. studies. Therefore, the lack of a pressure dependence in k_1(298 K,M) is most likely a consequence of the overall precision of their measurements. Tyndall et al.[11] also reported k_1(298 K,M) in the low-pressure regime with a constant value of (7 ± 2) × 10^{-13} cm^3 molecule^{-1} s^{-1} between 0.1 and 2 Torr (N$_2$). In the Tyndall et al. study, k_1(298 K,M) was determined relative to the CH$_3$CO + Cl$_2$ reaction. Gierczak et al.[32] have since reported the CH$_3$CO + Cl$_2$ rate coefficient to be (2.2 ± 0.8) × 10^{-11} exp((85 ± 120)/T) cm^3 molecule^{-1} s^{-1} and (3.0 ± 0.5) × 10^{-11} cm^3 molecule^{-1} s^{-1} at 296 K. (See Table 6 for revised and scaled values from the Tyndall et al. study.) Although the revised rate coefficient is in reasonable agreement with the present VLPR determination, there remains considerable uncertainty in the value determined using the relative rate method due to the present level of uncertainty in the reference reaction rate coefficient. Tyndall et al. also reported k_1(228 K,M) data in the low-pressure regime with an increase of 20 to 30% in k_1(228 K,M) over k_1(298 K,M) reported over the pressure range 0.1 to 2 Torr, which corresponds to a negative temperature dependence with an E/R of approximately −200 K. A negative temperature dependence is consistent with the interpretation of the present results, although their |E/R| value is substantially less than that obtained in the present work.

Tyndall et al.,[11] Kaiser and Wallington,[36] Sehested et al.,[10] Blitz et al.,[5,6] Romero et al.,[37] and Carr et al.[7] have reported k_1(298 K,M) data at pressures >10 Torr. The results from these studies are included in Table 6 and plotted in Figures 6 and 7 for comparison with the present results. The studies from the Leeds group (Blitz et al.,[5,6] Romero et al.,[37] and Carr et al.[7]) covered a range of temperature and pressure and were combined in their most recent Carr et al.[7] publication. Overall, the agreement among the various studies is reasonable, although the scatter among the literature data is greater than the precision obtained in the present work.

Kaiser and Wallington[36] and Sehested et al.[10] reported k_1(298 K,M) values at near atmospheric pressure. Kaiser and Wallington[36] studied reaction 1 in an environmental chamber at 296 K and 700 Torr relative to the CH$_3$CO + Cl$_2$ reaction by monitoring the formation of stable end-products. Using the CH$_3$CO + Cl$_2$ reaction rate coefficient from Gierczak et al.[32] and their reported reaction rate coefficient ratio results in k_1(298 K, 700 Torr (N$_2$)) = (3.8 ± 0.25) × 10^{-12} cm^3 molecule^{-1} s^{-1}. Their result falls below all other results performed at similar total pressures. Sehested et al.[10] used a pulsed radiolysis transient UV absorption technique to monitor the formation of CH$_3$C(O)O$_2$ in reaction 1 and determined an absolute value for k_1(295 K, 1000 mbar (SF$_6$)). The use of 1000 mbar of SF$_6$ bath gas enabled the measurement to better approach the high-pressure limit for reaction 1. A rate coefficient of (4.4 ± 0.7) × 10^{-12} cm^3 molecule^{-1} s^{-1} was reported, which is reasonably consistent with the present analysis.

Tyndall et al.[11] and the Leeds group[7] have reported k_1(T,M) over a range of pressure and temperature with He and N$_2$ bath gases. The falloff behavior parametrization reported in the Tyndall et al. work is given in Table 6, and the calculated rate coefficients are included in Figure 7. While the parametrization yields rate coefficient data in reasonable agreement with the present results at low pressure (after scaling to account for the most recent determination of the CH$_3$CO + Cl$_2$ rate coefficient), there is a significant systematic difference observed at higher pressures. The experimental data from the Leeds

group are included in Figures 6 and 7. In general, the Leeds $k_1(298\ K,M)$ data are lower than those obtained in the present work and display a higher level of scatter. The falloff parameters reported in Carr et al.[7] are given in Table 6. Their fit parametrization returned a low-pressure rate coefficient of 1.47×10^{-12} cm^3 molecule^{-1} s^{-1}, which is significantly greater than obtained in our VLPR experiments and reported in the Tyndall et al.[11] and Kovács et al.[8] studies. As previously mentioned, fitting the experimental data does not necessarily yield a unique set of falloff parameters, and not constraining the fit to an experimental low-pressure rate coefficient, as done in the present work, impacts the returned falloff parameters. Their high-pressure limit rate coefficient is also greater than obtained in the other literature studies. The third body efficiency for He relative to N$_2$ bath gas was found to be 0.61 ± 0.08, which is consistent with the present results.

5.1. OH Yield. Michael et al.[38] observed evidence of OH radical generation in reaction 1 in their 1985 low-pressure discharge flow study of the OH + CH$_3$CHO reaction in the presence of O$_2$. Since then, the determination of the temperature and pressure dependence of the OH radical yield in reaction 1 has been the focus of a number of experimental studies, although the agreement among these studies is not particularly good. The results from the present study are compared with these studies here.

OH yields have been determined experimentally using a variety of approaches that include both direct and indirect methods.

Kinetic Method. In this method, experimental $k_1(T,M)$ data obtained over a range of temperature and pressure are interpreted using a chemical activation reaction mechanism (Scheme 1). This method was employed in the studies by Tyndall et al.,[11] the Leeds group,[7] and in the present work, each using their own experimental data. This method requires precise kinetic data, particularly including data in the low-pressure regime.

Regeneration Method. In this method, OH radical decay temporal profiles are measured following the formation of CH$_3$CO radicals in the absence and presence of excess O$_2$. The relative difference in the measured OH decay pseudo-first order rate coefficient is directly related to $Y(T,M)$. This method was used in the Kovács et al.[8] study.

Internal Calibration Method. In this method, OH and CH$_3$CO radicals are produced either chemically or photolytically with known stoichiometry. The initial OH signal and the increase in the OH signal following reaction 1 are measured. An advantage of this method is that an absolute calibration of the system OH sensitivity is not required. Carr et al.[34] have employed this method.

Absolute Method. In this method, the yield of the OH radical in reaction 1 is measured using a calibrated OH detection method. An accurate calibration of the system OH sensitivity is required and often accomplished in pulsed laser photolysis systems using actinometry methods. The OH yield pressure dependence has often been interpreted using a Stern–Volmer analysis, which is discussed further later. This method has been applied in the Groß et al.[35] study.

Relative Method. In this method, the relative pressure dependence of the OH yield is measured. Absolute yields are obtained by scaling the measured values to an independently determined or assumed value. This method has been used by the Leeds group.[7]

The OH yield data from the previous studies are compared with the profiles obtained in the present study using the kinetic method for He and N$_2$ bath gases in Figures 6 and 7. The agreement among the previous studies is poor over the 1 to 50 Torr pressure range. In particular, OH yield results from the Leeds group, although self-consistent, are significantly greater than results reported in all other studies. The methods used and a comparison of the previous studies with the present OH yield determination are discussed later.

First, a Stern–Volmer (SV) analysis has been used in several of the literature studies and warrants further consideration. Invoking a simple Lindemann mechanism to reaction 1

$$Y(M) = \frac{k_{OH}}{(k_{OH} + k_{CH_3C(O)O_2}[M])} \tag{XXI}$$

and SV analysis

$$\frac{1}{Y(M)} = 1 + \frac{k_{CH3C(O)O_2}}{k_{OH}}[M] \tag{XXII}$$

has been used in the analysis of the OH yield pressure dependence. This analysis assumes that the k_{OH} and $k_{CH3C(O)O_2}$ are independent, which is not the case for Scheme 1; see eq XX and the discussion in Tyndall et al.,[11] which show that k_{bi} and k_{ter} are correlated with opposite dependences on pressure. In the $F_c = 1$ limit, the SV and kinetic method analysis would yield the same OH yield. An SV analysis applied with $F_c < 1$ would lead to a systematic overestimate of the OH yield. The SV and kinetic method analysis also lead to different ratios of the N$_2$ and He collision efficiencies. The literature SV analysis reports a N$_2$/He collision efficiency ratio of ~2.7, while the kinetic method presented here and by Carr et al.[7] reports a ratio between 1.3 and 1.6.

Kinetic Method. Accounting for the falloff behavior in this method has been outlined in detail in Tyndall et al.[11] and reviewed in this paper. A critical parameter in the OH yield analysis for reaction 1 is the accuracy of k_{int}. As shown in Figures 6 and 7, the uncertainty in k_{int} propagates throughout the OH yield pressure-dependent profile. The situation where k_{int} is not well-established experimentally and only determined from a fit of the falloff behavior leads to increased uncertainty in $Y(T,M)$, particularly in the low-pressure regime.

The OH yields obtained from the scaled Tyndall et al.[11] $k_1(T,M)$ data (measured over the pressure range 0.1 to 1000 Torr (N$_2$)) intersect the present results with systematic differences observed in the high- and low-pressure limits of the data. The OH yields reported by the Leeds group are substantially higher than reported in this and other studies. Although, there are systematic differences between the values of $k_1(T,M)$ measured in this work and the Leeds group, the greater value of k_{int} obtained in the Leeds group data analysis is primarily responsible for their greater calculated $Y(T,M)$ values. Our low-pressure VLPR rate coefficient measurement suggests that the Leeds group OH yield data are systematically overestimated. Note also that it is difficult to reproduce the Leeds $k_1(T,M)$ experimental values very well with a $k_{int}(296\ K)$ value much greater than our estimated uncertainty limit. Constraining a fit of the Leeds group data to our k_{int} value brings the OH yields from the two studies into better agreement, where approximately half of the difference, ~20%, is accounted for at 10 Torr (He). The remaining difference in

the OH yield is due to the differences in the high-pressure rate coefficient data.

Regeneration Method. Kovács et al.[8] determined pressure-dependent OH yields in reaction 1 at 296 K over the pressure range 1 to 10 Torr (He). In their discharge-flow tube experiment, pseudo-first-order OH loss rate coefficients, k', were measured following the formation of the CH_3CO radical in the $OH + CH_3CHO$ reaction in the presence and absence of excess O_2. The rapid regeneration of the OH radical in reaction 1 (excess O_2) decreases the observed OH loss, and the OH yield is given by

$$Y(296\ K,\ M) = \frac{k' - k'_{O_2}}{k'} \tag{XXIII}$$

Although Kovács et al.[8] did not observe a measurable change in $k_1(296\ K,M)$ between 1 and 10 Torr (He), they did observe a significant OH yield pressure dependence, as shown in Figure 6. In this method, it is necessary to keep the $[O_2]/[CH_3CHO]$ ratio large to avoid systematic errors in the OH yield. (The CH_3CHO concentration determines the rate of CH_3CO radical production in the Kovács et al. study.). The typical conditions stated in the Kovács et al. study of $[O_2]/[CH_3CHO] = 50$ would result in only a small, ∼2%, overestimate of the OH yield. The range of concentrations used in the study could, however, lead to larger error; for example, a ratio of 20 would have a 12% error. The OH yields obtained in the Kovács et al. study are systematically greater than the values determined in this work by ∼25%, which falls near the combined uncertainties of our two studies.

Note that the OH yields reported from our laboratory by Talukdar et al. at the 2006 International Symposium on Gas Kinetics and cited in previous studies also used this method. Their results are in reasonable agreement with the present kinetic method analysis.

Internal Calibration Method. Carr et al.[7] is the only study to date that has applied the internal calibration method to the measurement of the OH yield in reaction 1. Pulsed laser photolysis of $CH_3C(O)OH$ at 248 nm

$$CH_3C(O)OH + h\nu \rightarrow CH_3CO + OH \tag{7a}$$

$$\rightarrow \text{other products} \tag{7b}$$

in the presence of O_2 was used to produce a 1:1 stoichiometric mixture of OH and CH_3CO radicals as primary photolysis products. The OH radical temporal profile was measured using LIF. The primary OH radical signal provides the internal standard, against which OH radical production from reaction 1 was measured. Measurements were performed at room temperature and 5−100 Torr (He) or 5−25 Torr (N_2) total pressure. The results are included in Figures 6 and 7. Their OH yields are significantly greater than obtained in the present work using the kinetic method. There is presently no apparent explanation for the difference between the two methods.

Absolute Method. Groß et al.[35] used 248 nm pulsed laser photolysis to produce CH_3CO radicals via the $Cl + CH_3CHO$ reaction (Cl atoms were produced by photolysis of Cl_2CO) and $CH_3C(O)CH_3$ photolysis. OH radicals were detected by LIF and quantified using the photolysis of H_2O_2. Groß et al. measured the OH yield at 298 K over the pressure range 27 to 400 mbar with He, N_2, and air bath gases. The OH yield was analyzed using the SV method, and the obtained k_{OH}/k_{CH3CO} for N_2 and He are $(9.4 \pm 1.7) \times 10^{-18}$ and $(3.6 \pm 0.6) \times 10^{-18}$ cm^3 molecule^{-1}, respectively. The results from this study are

included in Figures 6 and 7. The results are in good agreement with the present kinetic method analysis. Note that the collision efficiency ratio for N_2 and He bath gas from the Groß et al. analysis is 2.6. This is significantly greater than the value obtained from the kinetic method analysis, even though the OH yields are in good agreement, as previously explained. Extrapolation of the Groß et al. SV analysis to lower pressure would also lead to erroneously higher OH yields than obtained in the present work.

6. SUMMARY AND CONCLUSIONS

Precise and accurate phenomenological rate coefficients for the gas-phase reaction of the CH_3CO radical with O_2 are reported in this work. Rate coefficients were measured using three independent experimental methods that cover the pressure range 0.009 to 600 Torr with N_2 and He bath gases at 241, 296, and 373 K. The rate coefficient displays complex bimolecular and termolecular falloff behavior under these conditions. The rate coefficient in the zero pressure limit was measured experimentally at 296 K to be $(9.94 \pm 1.32) \times 10^{-13}$ cm^3 molecule^{-1} s^{-1}.

Our rate coefficient data were interpreted using a chemical activation mechanism (Scheme 1) to determine the pressure and temperature dependence, that is, falloff behavior, of the bimolecular (OH radical channel) and termolecular ($CH_3C(O)O_2$ radical channel) reaction channels. The experimental data were reproduced very well with the chemical activation mechanism and falloff parameters using the Troe formalism with the fit results given in Table 5. The OH yield is small at atmospheric pressure, ∼1 to 2%, and increases at lower pressures; for example, at 296 K the OH yield is 0.19 and 0.81 at 25 and 1 Torr (He), respectively. On the basis of the kinetic analysis presented in this work, the OH yield was determined to have a weak temperature dependence; however, the determination of the OH yield temperature dependence is sensitive to the temperature dependence of the bimolecular rate coefficient in the zero pressure limit, that is, $k_{int}(T)$, which in this work was inferred from the fitting of $k_1(T,M)$ at higher pressures. Direct experimental measurements of $k_{int}(T)$ over a range of temperatures would help constrain the OH yield temperature dependence.

The total rate coefficient for reaction 1 and the OH radical yields for the $CH_3CO + O_2$ reaction obtained in this work were critically compared with previously reported literature values. Overall, the agreement is reasonable, although the OH yields reported by Carr et al.[34] using the "internal calibration method" are inexplicably systematically higher than values reported in all other studies.

■ AUTHOR INFORMATION

Corresponding Author

*E-mail: James.B.Burkholder@noaa.gov. Tel: 303-497-3252.

Present Addresses

∥V.C.P.: Laboratory of Photochemistry and Chemical Kinetics, Department of Chemistry, University of Crete, Vassilika Vouton, 71003, Heraklion, Crete, Greece.

⊥T.G.: Department of Chemistry, Warsaw University, al. Żwirki i Wigury 101, 02-089 Warszawa, Poland.

Notes

The authors declare no competing financial interest.

■ REFERENCES

(1) Barker, J. R.; Golden, D. M. Master Equation Analysis of Pressure-Dependent Atmospheric Reactions. *Chem. Rev.* **2003**, *103*, 4577−4591.

(2) Sander, S. P.; Abbatt, J.; Barker, J. R.; Burkholder, J. B.; Friedl, R. R.; Golden, D. M.; Huie, R. E.; Kolb, C. E.; Kurylo, M. J.; Moortgat, G. K.; et al. *Chemical Kinetics and Photochemical Data for Use in Atmospheric Studies*; Evaluation Number 17, JPL Publication 10-6; Jet Propulsion Laboratory, California Institute of Technology: Pasadena, CA, 2011. http://jpldataeval.jpl.nasa.gov.

(3) Roberts, J. M. The Atmospheric Chemistry of Organic Nitrates. *Atmos. Environ.* **1990**, *24A*, 243−287.

(4) Talukdar, R. K.; Burkholder, J. B.; Schmoltner, A.-M.; Roberts, J. M.; Wilson, R. R.; Ravishankara, A. R. Investigation of the Loss Processes for Peroxyacetyl Nitrate in the Atmosphere: UV Photolysis and Reaction with OH. *J. Geophys. Res.* **1995**, *100*, 14163−14173.

(5) Blitz, M. A.; Heard, D. E.; Pilling, M. J. OH Formation from $CH_3CO + O_2$: A Convenient Experimental Marker for the Acetyl Radical. *Chem. Phys. Lett.* **2002**, *365*, 374−379.

(6) Blitz, M. A.; Heard, D. E.; Pilling, M. J.; Arnold, S. R.; Chipperfield, M. P. Pressure and Temperature-Dependent Quantum Yields for the Photodissociation of Acetone Between 279 and 327.5 nm. *Geophys. Res. Lett.* **2004**, *31*, L06111.

(7) Carr, S. A.; Glowacki, D. R.; Liang, C.-H.; Baeza-Romero, M. T.; Blitz, M. A.; Pilling, M. J.; Seakins, P. W. Experimental and Modeling Studies of the Pressure and Temperature Dependences of the Kinetics and the OH Yields in the Acetyl O_2 Reaction. *J. Phys. Chem. A* **2011**, 1069−1085.

(8) Kovács, G.; Zádor, J.; Farkas, E.; Nádasdi, R.; Szilágyi, I.; Dóbé, S.; Bérces, T.; Márta, F.; Lendvay, G. Kinetics and Mechanism of the Reactions of CH_3CO and $CH_3C(O)CH_2$ Radicals with O_2. Low-Pressure Discharge Flow Experiments and Quantum Chemical Computations. *Phys. Chem. Chem. Phys.* **2007**, *9*, 4142−4154.

(9) McDade, C. E.; Lenhardt, T. M.; Bayes, K. D. The Rate of Reaction of Acetyl and Benzoly Radicals with O_2. *J. Photochem.* **1982**, *20*, 1−7.

(10) Sehested, J.; Christensen, L. K.; Nielsen, O. J.; Wallington, T. J. Absolute Rate Constants for F + CH_3CHO and $CH_3CO + O_2$, Relative Rate Study of CH_3CO + NO, and the Product Distribution of the F + CH_3CHO Reaction. *Int. J. Chem. Kinet.* **1998**, *30*, 913−921.

(11) Tyndall, G. S.; Orlando, J. J.; Wallington, T. J.; Hurley, M. D. Pressure Dependence of the Rate Coefficients and Product Yields for the Reaction of CH_3CO Radicals with O_2. *Int. J. Chem. Kinet.* **1997**, *29*, 655−663.

(12) Tyndall, G. S.; Staffelbach, T. A.; Orlando, J. J.; Calvert, J. G. Rate Coefficients for the Reactions of OH Radicals with Methylglyoxal and Acetaldehyde. *Int. J. Chem. Kinet.* **1995**, *27*, 1009−1020.

(13) Maranzana, A.; Barker, J. R.; Tonachini, G. Master Equation Simulations of Competing Unimolecular and Bimolecular Reactions: Application to OH Production in the Reaction of Acetyl Radical with O_2. *Phys. Chem. Chem. Phys.* **2007**, *9*, 4129−4141.

(14) Baasandorj, M.; Knight, G.; Papadimitriou, V. C.; Talukdar, R. K.; Ravishankara, A. R.; Burkholder, J. B. Rate Coefficients for the Gas-Phase Reaction of the Hydroxyl Radical with $CH_2=CHF$ and $CH_2=CF_2$. *J. Phys. Chem. A* **2010**, *114*, 4619−4633.

(15) Papadimitriou, V. C.; Talukdar, R. K.; Portmann, R. W.; Ravishankara, A. R.; Burkholder, J. B. $CF_3CF=CH_2$ and (Z)-$CF_3CF=CHF$: Temperature Dependent OH Rate Coefficients and Global Warming Potentials. *Phys. Chem. Chem. Phys.* **2008**, *10*, 808−820.

(16) Rajakumar, B.; Flad, J. E.; Gierczak, T.; Ravishankara, A. R.; Burkholder, J. B. Visible Absorption Spectrum of the CH_3CO Radical. *J. Phys. Chem. A* **2007**, *111*, 8950−8958.

(17) Rajakumar, B.; Gierczak, T.; Flad, J. E.; Ravishankara, A. R.; Burkholder, J. B. The CH_3CO Quantum Yield in the 248 nm Photolysis of Acetone, Methyl Ethyl Ketone, and Biacetyl. *J. Photochem. and Photobio, A: Chem.* **2008**, *199*, 336−344.

(18) Papadimitriou, V. C.; Papanastasiou, D. K.; Stefanopoulos, V. G.; Zaras, A. M.; Lazarou, Y. G.; Papagiannakopoulos, P. Kinetic Study of the Reactions of Cl Atoms with $CF_3CH_2CH_2OH$, $CF_3CF_2CH_2OH$, $CHF_2CF_2CH_2OH$, and $CF_3CHFCF_2CH_2OH$. *J. Phys. Chem. A* **2007**, *111*, 11608−11617.

(19) Papadimitriou, V. C.; Prosmitis, A. V.; Lazarou, Y. G.; Papagiannakopoulos, P. Absolute Reaction Rates of Chlorine Atoms with CF_3CH_2OH, CHF_2CH_2OH, and CH_2FCH_2OH. *J. Phys. Chem. A* **2003**, *107*, 3733−3740.

(20) Romanias, M. N.; Zogka, A. G.; Papadimitriou, V. C.; Papagiannakopoulos, P. Uptake Measurements of Acetic Acid on Ice and Nitric Acid-Doped Thin Ice Films over Upper Troposphere/Lower Stratosphere Temperatures. *J. Phys. Chem. A* **2012**, *116*, 2198−2208.

(21) Romanias, M. N.; Zogka, A. G.; Stefanopoulos, V. G.; Papadimitriou, V. C.; Papagiannakopoulos, P. Uptake of Formic Acid on Thin Ice Films and on Ice Doped with Nitric Acid between 195 and 211 K. *ChemPhysChem* **2010**, *11*, 4042−4052.

(22) Stefanopoulos, V. G.; Papadimitriou, V. C.; Lazarou, Y. G.; Papagiannakopoulos, P. Absolute Rate Coefficient Determination and Reaction Mechanism Investigation for the Reaction of Cl Atoms with CH_2I_2 and the Oxidation Mechanism of CH_2I Radicals. *J. Phys. Chem. A* **2008**, *112*, 1526−1535.

(23) Gierczak, T.; Burkholder, J. B.; Bauerle, S.; Ravishankara, A. R. Photochemistry of Acetone under Tropospheric Conditions. *Chem. Phys.* **1998**, *231*, 229−244.

(24) Khamaganov, V.; Karunanandan, R.; Rodriguez, A.; Crowley, J. N. Photolysis of $CH_3C(O)CH_3$ (248 nm, 266 nm), $CH_3C(O)C_2H_5$ (248 nm) and $CH_3C(O)Br$ (248 nm): Pressure Dependent Quantum Yields of CH_3 Formation. *Phys. Chem. Chem. Phys.* **2007**, *9*, 4098−4113.

(25) Nádasdi, R.; Kovács, G.; Szilágyi, I.; Demeter, A.; Dóbé, S.; Bérces, T.; Márta, F. Exciplex Laser Photolysis Study of Acetone with Relevance to Tropospheric Chemistry. *Chem. Phys. Lett.* **2007**, *440*, 31−35.

(26) Emrich, M.; Warneck, P. J. Photodissociation of Acetone in Air: Dependence on Pressure and Wavelength. Behavior of the Excited Singlet State. *J. Phys. Chem. A* **2000**, *104*, 9436−9442.

(27) NIST Chemical Kinetics Database, 2014. http://kinetics.nist.gov.

(28) Ammann, M.; Cox, R. A.; Crowley, J. N.; Jenkin, M. E.; Mellouki, A.; Rossi, M. J.; Troe, J.; Wallington, T. J. IUPAC Task Group on Atmospheric Chemical Kinetic Data Evaluation, 2014. http://iupac.pole-ether.fr.

(29) Niki, H.; Maker, P. D.; Savage, C. M.; Breitenbach, L. P. FTIR Study of the Kinetics and Mechanism for Cl-Atom-Initiated Reactions of Acetaldehyde. *J. Phys. Chem.* **1985**, *89*, 588−591.

(30) Bartels, M.; Hoyermann, K.; Lange, U. An Experimental Study of the Reactions of CH_3CHO + Cl, C_2H_4O + Cl, and C_2H_4O + F in the Gas Phase. *Ber. Bunsen-Ges.* **1989**, *93*, 423−427.

(31) Brown, S. S.; Ravishankara, A. R.; Stark, H. Simultaneous Kinetics and Ring-Down: Rate Coefficients from Single Cavity Loss Temporal Profiles. *J. Phys. Chem. A* **2000**, *104*, 7044−7052.

(32) Gierczak, T.; Rajakumar, B.; Flad, J. E.; Burkholder, J. B. Rate Coefficients for the Reaction of the Acetyl Radical, CH_3CO, with Cl_2 between 253 and 384 K. *Int. J. Chem. Kinet.* **2009**, *41*, 543−553.

(33) Zhu, L.; Johnston, G. Kinetics and Products of the Reaction of the Vinoxy Radical with O_2. *J. Phys. Chem.* **1995**, *99*, 15114−15119.

(34) Carr, S. A.; Baeza-Romero, M. T.; Blitz, M. A.; Pilling, M. J.; Heard, D. E.; Seakins, P. W. OH Yields from the $CH_3CO + O_2$ Reaction Using an Internal Standard. *Chem. Phys. Lett.* **2007**, *445*, 108−112.

(35) Groß, C. B. M.; Dillon, T. J.; Crowley, J. N. Pressure Dependent OH Yields in the Reactions of CH_3CO and $HOCH_2CO$ with O_2. *Phys. Chem. Chem. Phys.* **2014**, *16*, 10990−10998.

(36) Kaiser, E. W.; Wallington, T. J. CH_3CO Reactions with Cl_2 and O_2: More Evidence for HCl Elimination from the CH_3CHClO Radical. *J. Phys. Chem.* **1995**, *99*, 8669−8672.

(37) Romero, M. T. B.; Blitz, M. A.; Heard, D. E.; Pilling, M. J.; Price, B.; Seakins, P. W. OH Formation from the $C_2H_5CO + O_2$ Reaction: An Experimental Marker for the Propionyl Radical. *Chem. Phys. Lett.* **2005**, *408*, 232−236.

(38) Michael, J. V.; Keil, D. G.; Klemm, R. B. Rate Constants for the Reaction of Hydroxyl Radicals with Acetaldehyde from 244−528 K. *J. Chem. Phys.* **1985**, *83*, 1630−1636.